

Glucose metabolism links astroglial mitochondria to cannabinoid effects

<https://doi.org/10.1038/s41586-020-2470-y>

Received: 9 March 2018

Accepted: 29 May 2020

Published online: 8 July 2020

 Check for updates

Daniel Jimenez-Blasco^{1,2,3,23}, Arnau Busquets-Garcia^{4,5,6,23}, Etienne Hebert-Chatelain^{7,8,23}, Roman Serrat^{4,5}, Carlos Vicente-Gutierrez^{1,2,3}, Christina Ioannidou^{4,5}, Paula Gómez-Sotres^{4,5}, Irene Lopez-Fabuel^{1,2,3}, Monica Resch-Beusher^{1,2,3}, Eva Resel^{9,10}, Dorian Arnouil^{4,5}, Dave Saraswat^{4,5}, Marjorie Varilh^{4,5}, Astrid Cannich^{4,5}, Francisca Julio-Kaljic^{4,5}, Itziar Bonilla-Del Río^{11,12}, Angeles Almeida^{1,3}, Nagore Puente^{11,12}, Svein Achicallende^{11,12}, Maria-Luz Lopez-Rodriguez¹³, Charlotte Jollé¹⁴, Nicole Déglon¹⁵, Luc Pellerin^{14,16,21}, Charlene Josephine¹⁷, Gilles Bonvento¹⁷, Aude Panatier^{4,5}, Beat Lutz^{18,19}, Pier-Vincenzo Piazza^{4,5,22}, Manuel Guzmán^{9,10}, Luigi Bellocchio^{4,5}, Anne-Karine Bouzier-Sore¹⁶, Pedro Grandes^{11,12,20}, Juan P. Bolaños^{1,2,3,24} ✉ & Giovanni Marsicano^{4,5,24} ✉

Astrocytes take up glucose from the bloodstream to provide energy to the brain, thereby allowing neuronal activity and behavioural responses^{1–5}. By contrast, astrocytes are under neuronal control through specific neurotransmitter receptors^{5–7}. However, whether the activation of astroglial receptors can directly regulate cellular glucose metabolism to eventually modulate behavioural responses is unclear. Here we show that activation of mouse astroglial type-1 cannabinoid receptors associated with mitochondrial membranes (mtCB₁) hampers the metabolism of glucose and the production of lactate in the brain, resulting in altered neuronal functions and, in turn, impaired behavioural responses in social interaction assays. Specifically, activation of astroglial mtCB₁ receptors reduces the phosphorylation of the mitochondrial complex I subunit NDUFS4, which decreases the stability and activity of complex I. This leads to a reduction in the generation of reactive oxygen species by astrocytes and affects the glycolytic production of lactate through the hypoxia-inducible factor 1 pathway, eventually resulting in neuronal redox stress and impairment of behavioural responses in social interaction assays. Genetic and pharmacological correction of each of these effects abolishes the effect of cannabinoid treatment on the observed behaviour. These findings suggest that mtCB₁ receptor signalling can directly regulate astroglial glucose metabolism to fine-tune neuronal activity and behaviour in mice.

The energy demands of astrocytes are almost exclusively met by glycolysis, whereas those of neurons mainly rely on oxidative phosphorylation (OXPHOS)⁸. In this context, mitochondrial complex I is assembled into supercomplexes to increase OXPHOS efficacy in neurons, whereas the majority of astroglial complex I is free, which results in low OXPHOS efficacy in these cells⁹. Thus, astrocytes produce higher levels of mitochondrial reactive oxygen species (mROS)⁹, which control the hypoxia-inducible factor (HIF) cascade and the expression of key

enzymes for the metabolism of glucose¹⁰. However, the potential effect of this molecular cascade on animal behaviour is unknown.

The type-1 cannabinoid receptor (CB₁) is the main target of Δ^9 -tetrahydrocannabinol (THC)—the psychoactive component of *Cannabis sativa*—and of other (endo)cannabinoids. CB₁ is widely expressed in the brain and regulates several behavioural responses¹¹. Whereas high levels of CB₁ are found in neurons that control many cannabinoid-induced effects, previous studies have underlined that

¹Institute of Functional Biology and Genomics, University of Salamanca, CSIC, Salamanca, Spain. ²Centro de Investigación Biomédica en Red sobre Fragilidad y Envejecimiento Saludable (CIBERFES), Instituto de Salud Carlos III, Madrid, Spain. ³Institute of Biomedical Research of Salamanca, University Hospital of Salamanca, University of Salamanca, CSIC, Salamanca, Spain. ⁴INSERM, U1215 NeuroCentre Magendie, Bordeaux, France. ⁵University of Bordeaux, Bordeaux, France. ⁶Integrative Pharmacology and Systems Neuroscience, IMIM Hospital del Mar Medical Research Institute, Barcelona, Spain. ⁷Canada Research Chair in Mitochondrial Signaling and Physiopathology, Université de Moncton, Moncton, New Brunswick, Canada. ⁸Department of Biology, Université de Moncton, Moncton, New Brunswick, Canada. ⁹Instituto Ramón y Cajal de Investigación Sanitaria (IRYCIS), Instituto Universitario de Investigación Neuroquímica (IUIN) and Department of Biochemistry and Molecular Biology, Complutense University, Madrid, Spain. ¹⁰Centro de Investigación Biomédica en Red sobre Enfermedades Neurodegenerativas (CIBERNED), Instituto de Salud Carlos III, Madrid, Spain. ¹¹Department of Neurosciences, University of the Basque Country (UPV/EHU), Leioa, Spain. ¹²Achucarro Basque Center for Neuroscience, Science Park of the UPV/EHU, Leioa, Spain. ¹³Department of Organic Chemistry, Complutense University, Madrid, Spain. ¹⁴Department of Physiology, University of Lausanne, Lausanne, Switzerland. ¹⁵Department of Clinical Neurosciences, Laboratory of Cellular and Molecular Neurotherapies (LCMN), University of Lausanne, Lausanne, Switzerland. ¹⁶Centre de Résonance Magnétique des Systèmes Biologiques UMR 5536, CNRS-University of Bordeaux, Bordeaux, France. ¹⁷Université Paris-Saclay, CEA, CNRS, MIRCen, Laboratoire des Maladies Neurodégénératives, Fontenay-aux-Roses, France. ¹⁸Institute of Physiological Chemistry, University Medical Center, Mainz, Germany. ¹⁹Leibniz Institute for Resilience Research (LIR), Mainz, Germany. ²⁰Division of Medical Sciences, University of Victoria, Victoria, British Columbia, Canada. ²¹Present address: INSERM U1082, University of Poitiers, Poitiers, France. ²²Present address: Aelis Farma, Bordeaux, France. ²³These authors contributed equally: Daniel Jimenez-Blasco, Arnau Busquets-Garcia, Etienne Hebert-Chatelain. ²⁴These authors jointly supervised this work: Juan P. Bolaños, Giovanni Marsicano. ✉e-mail: jbolanos@usal.es; giovanni.marsicano@inserm.fr

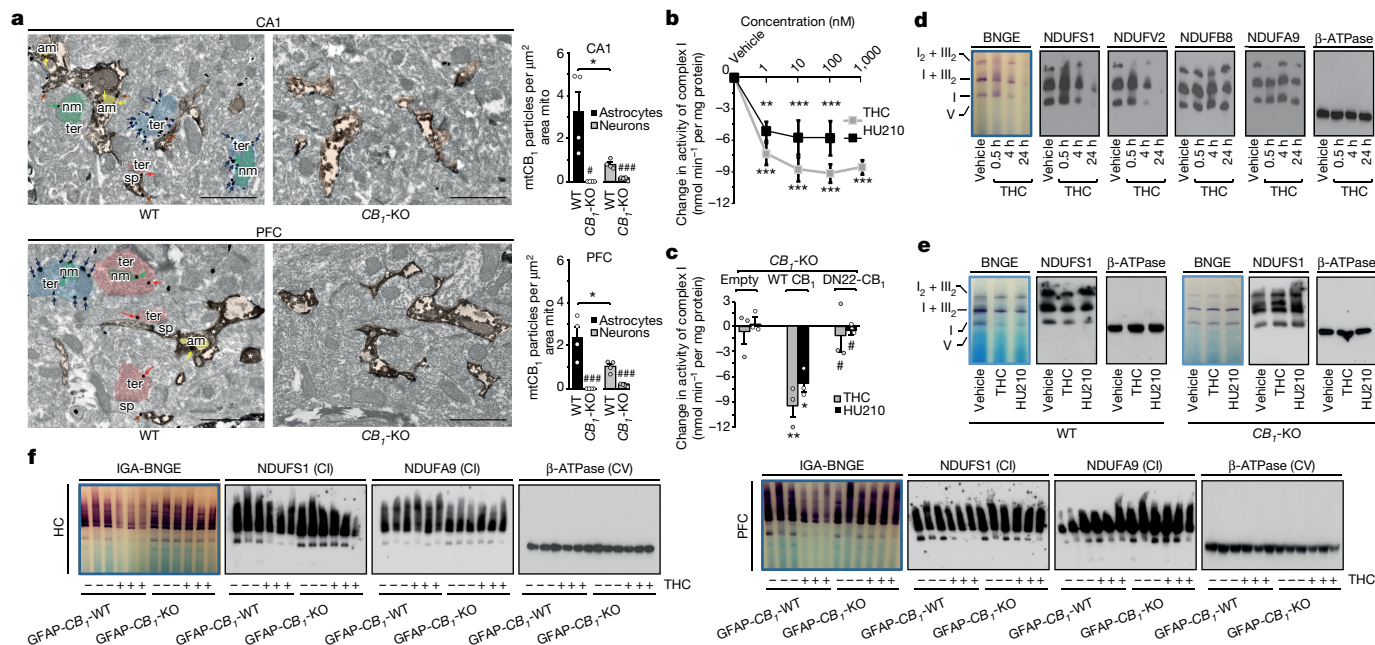


Fig. 1 mtCB₁ activation inhibits the activity of complex I by destabilization of the N-module. **a**, Left, detection of CB₁ receptors on mitochondrial membranes of astroglia and neurons in the hippocampus (CA1 region) and the PFC of wild-type and *CB₁*-KO mice (*n* = 4 mice). am, astrocytic mitochondria; nm, neuronal mitochondria; sp, spine; ter, terminal. CB₁-positive inhibitory terminals are marked in blue, astrocytes in brown, excitatory terminals in red, astrocytic mitochondria in yellow and neuronal mitochondria in green. Asterisks indicate astrocytic processes; coloured arrows point to CB₁ particles at colour-matching subcellular compartments and mitochondria. Scale bars, 1 μm. Right, quantification of mtCB₁ on mitochondrial membranes (mean ± s.e.m.). *P* values by one-way analysis of variance (ANOVA); **P* < 0.05 (wild-type astrocytic versus wild-type neuronal mitochondria); #*P* < 0.05, ###*P* < 0.001 (wild type versus *CB₁*-KO). **b**, Change in the activity of complex I in wild-type astrocytes when treated with THC (1 μM) or HU210 (50 nM). **c**, Change in the activity of complex I in *CB₁*-KO astrocytes that were transfected with empty vector or with plasmids that express wild-type CB₁ or DN22-CB₁, and treated with THC (1 μM) or HU210 (50 nM). Data in **b, c** are expressed as the

normalized baseline change in complex I activity (mean ± s.e.m.); **b**, 22.9 ± 1.3 nmol min⁻¹ per mg protein; **c**, 26.6 ± 1.4, 23.7 ± 2.2 and 21.3 ± 2.7 nmol min⁻¹ per mg protein for empty vector, wild-type CB₁ and CB₁-DN22, respectively. *P* values by one-way ANOVA; **P* < 0.05, ***P* < 0.01, ****P* < 0.001 (versus vehicle); #*P* < 0.05 (versus wild-type CB₁). *n* = 3 independent experiments (**b, c**); Methods. **d**, Effects of THC treatment for the indicated times on the activity of complex I (measured by blue native gel electrophoresis (BNGE)) and the expression of NDUFS1, NDUFV2, NDUFB8, NDUFA9 and β-ATPase in wild-type astrocytes. **e**, Effects of THC or HU210 treatment on the activity of complex I (BNGE) and the expression of NDUFS1 and β-ATPase in wild-type or *CB₁*-KO astrocytes. **f**, Effects of THC treatment (10 mg kg⁻¹) on the activity of complex I (measured by in-gel NADH dehydrogenase activity (IGA) after BNGE; IGA-BNGE) and the expression of NDUFS1, NDUFA9 and β-ATPase in the hippocampus (HC) and PFC of GFAP-*CB₁*-WT and GFAP-*CB₁*-KO mice. CI, complex I; CV, complex V. For original gels, see Supplementary Fig. 1; for statistical details, see Supplementary Table 1.

astroglial CB₁ modulates the communication between astrocytes and neurons at the synaptic and behavioural level^{11–13}. The presence of functional mtCB₁ in different tissues, including the brain, underlies the contribution of cannabinoid signalling to bioenergetic processes^{14–19}. By modulating several mitochondrial functions, brain mtCB₁ affects synaptic transmission and behaviour¹⁵. However, whether astroglial mtCB₁ and the associated bioenergetic processes can affect behavioural responses has not yet been investigated.

Astroglial mtCB₁ regulates brain OXPHOS

In addition to the presence of mtCB₁ in neurons^{14,15,18,20}, CB₁ protein was specifically detected in close juxtaposition to astroglial mitochondria in the mouse hippocampus¹⁹, prefrontal cortex, piriform cortex and nucleus accumbens (Fig. 1a, Extended Data Fig. 1a). The cell-permeable CB₁ receptor agonist 1,1-dimethylheptyl-11-hydroxy-Δ⁸-tetrahydrocannabinol (HU210), but not a cell-impermeable biotinylated version of HU210 (HU210-biotin)¹⁴, reduced oxygen consumption in cultured mouse astrocytes (Extended Data Fig. 1b), suggesting that intracellular CB₁ is required for this effect of HU210. Activation of mtCB₁ reduces the mitochondrial activity of soluble adenylyl cyclase and the protein kinase A (PKA)-dependent phosphorylation of OXPHOS proteins¹⁵. Treatment with KH7, an inhibitor of soluble adenylyl cyclase, abolished the effect of HU210 on oxygen

consumption in cultures of mouse astrocytes (Extended Data Fig. 1c). The reduction in respiration that was induced by the CB₁ agonists THC and WIN55,212-2 (WIN) in purified mitochondria from whole brains of wild-type mice^{14,15} was abolished both in *CB₁*-knockout (KO) mice, which lack the *CB₁* gene (also known as *Cnr1*) globally, and in conditional mutant mice that lack *CB₁* specifically in cells (mainly astrocytes) that express glial fibrillary acidic protein (GFAP) (GFAP-*CB₁*-KO mice)²¹ (Extended Data Fig. 1d, e). Thus, astrocytes contain functional mtCB₁ receptors.

MtCB₁ destabilizes complex I

To ascertain whether astroglial mtCB₁ controls mitochondrial bioenergetics, cultured mouse astrocytes were incubated for 24 h with THC or HU210, which reduced the activity of complex I (Fig. 1b), but not that of other OXPHOS complexes or citrate synthase (Extended Data Fig. 2a), in a dose-dependent manner. To investigate the specific involvement of mtCB₁, we transfected astrocytes derived from *CB₁*-KO mice with plasmids that express either wild-type CB₁ or DN22-CB₁—a mutant form of CB₁ that is functional but is excluded from the mitochondria¹⁵. Re-expression of wild-type CB₁, but not DN22-CB₁, rescued the effect of THC and HU210 on the activity of complex I (Fig. 1c). As the structural conformation of complex I is pivotal to its enzymatic activity^{22,23}, we next assessed its stability. Treatment with THC or HU210

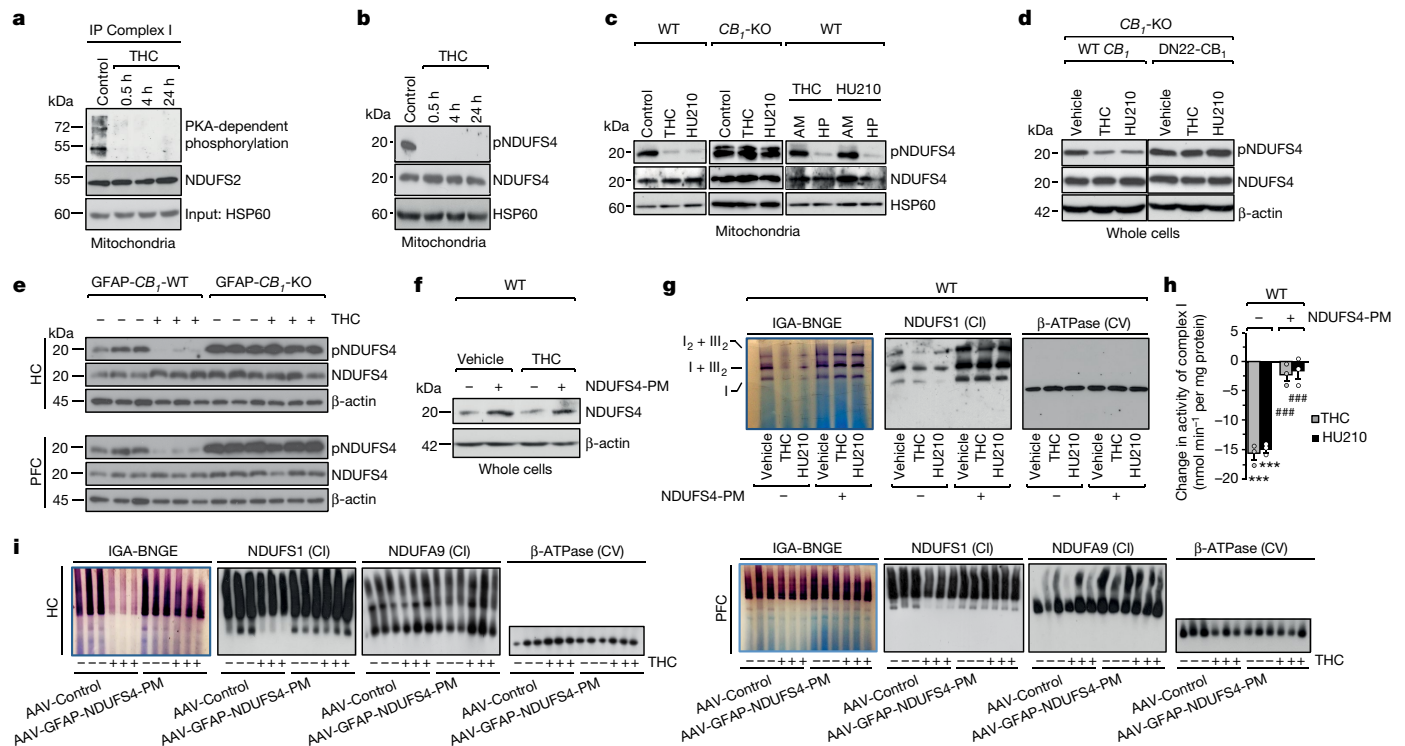


Fig. 2 | Astroglial mtCB₁ activation decreases the level of phosphorylated NDUFS4 and inhibits the activity of complex I. **a, b,** Effects of THC treatment (1 μM) for the indicated times on PKA-mediated phosphorylation and NDUFS2 expression in complex I-immunoprecipitated (IP) proteins (**a**) and on the levels of phosphorylated NDUFS4 (pNDUFS4) (**b**) in isolated mitochondria from wild-type astrocytes. **c,** Effects of THC (1 μM) or HU210 (50 nM) treatment on the levels of pNDUFS4 in mitochondria from wild-type astrocytes (left), *CB₁*-KO astrocytes (middle) or wild-type astrocytes in the presence of 1 μM AM251 (AM) or 10 μM haemopressin (HP) (right). **d,** Effects of THC or HU210 treatment on pNDUFS4 in *CB₁*-KO astrocytes that were transfected with plasmids that express wild-type *CB₁* or DN22-*CB₁*. **e,** Effects of THC treatment (10 mg kg⁻¹) on pNDUFS4 in the hippocampus and PFC of *GFAP-CB₁*-WT and *GFAP-CB₁*-KO mice.

f, Expression of NDUFS4-PM in wild-type astrocytes treated with THC. **g,** Effects of NDUFS4-PM expression on the activity of complex I and the expression of NDUFS1 and β-ATPase in wild-type astrocytes after treatment with vehicle, THC or HU210. **h,** Effects of THC or HU210 treatment on the activity of complex I in astrocytes that were transfected with empty vector or that express NDUFS4-PM. Data are mean ± s.e.m. (*n* = 3 independent experiments). *P* values by one-way ANOVA; *****P* < 0.001 (versus control conditions); ###*P* < 0.001 (versus empty vector). **i,** Effects of NDUFS4-PM expression in astrocytes of the hippocampus and PFC on the THC-induced decrease of complex I activity and NDUFS1 or NDUFA9 expression. HSP60 and β-actin were used as loading controls (**a–f**). For original gels, see Supplementary Fig. 1; for statistical details, see Supplementary Table 1.

reduced the activity of complex I in cultured astrocytes in a time- and *CB₁*-dependent manner, as well as decreasing the protein abundance of NDUFS1 and NDUFS2—which are subunits of the N-module of the matrix arm of complex I^{22,23}—but not that of NDUFB8 and NDUFA9, which are subunits of the inner-membrane-embedded P-module^{22,23} (Fig. 1d, e, Extended Data Fig. 2b–e). Administration of THC (10 mg per kg body weight by intraperitoneal injection) induced a destabilization of complex I in the hippocampus and prefrontal cortex (PFC) of *GFAP-CB₁*-WT mice (that is, wild-type littermates of *GFAP-CB₁*-KO)—but not of *GFAP-CB₁*-KO mice—24 h after injection, with a decrease in the abundance of the N-module NDUFS1 and NDUFS2 subunits but not the P-module NDUFA9 subunit (Fig. 1f, Extended Data Fig. 2f, g). Thus, *in vitro* and *in vivo* pharmacological activation of astroglial *CB₁* receptors causes a selective degradation of the N-module of complex I, which is responsible for the binding and oxidation of NADH(H⁺)^{22,23}.

MtCB₁ reduces the phosphorylation of NDUFS4

We next investigated the signalling mechanism that leads to complex I instability. Incubation with THC rapidly and persistently inhibited PKA-mediated phosphorylation of complex I proteins in cultured astrocytes, without affecting the Q-module NDUFS2 subunit (Fig. 2a, Extended Data Fig. 3a). As phosphorylation of the NDUFS4 subunit at Ser173 (NDUFS4-Ser173) determines the stability and assembly of the N-module of complex I²⁴, we next assessed whether stimulation of the

CB₁ receptor alters this phosphorylation site in astrocytes. Treatment with THC or HU210 decreased the phosphorylation of NDUFS4-Ser173 in astrocytes from wild-type mice, but not *CB₁*-KO mice (Fig. 2b, c, Extended Data Fig. 3b, c). This effect was blocked by the cell-permeable *CB₁* antagonist AM251, but not the cell-impermeable antagonist haemopressin¹⁴ (Fig. 2c, Extended Data Fig. 3c). Re-expression of *CB₁*, but not DN22-*CB₁*, in *CB₁*-KO astrocytes rescued the effects of THC and HU210 on NDUFS4-Ser173 phosphorylation (Fig. 2d, Extended Data Fig. 3d). Both hippocampus and PFC samples of THC-treated *GFAP-CB₁*-WT mice showed a strong reduction of NDUFS4-Ser173 phosphorylation (Fig. 2e, Extended Data Fig. 3e). Basal NDUFS4-Ser173 phosphorylation was higher in *GFAP-CB₁*-KO mice than in *GFAP-CB₁*-WT littermates (Fig. 2e, Extended Data Fig. 3e). However, the effect of THC was abolished in the mutant mice (Fig. 2e, Extended Data Fig. 3e). Thus, NDUFS4-Ser173 dephosphorylation involves the activation of astroglial *CB₁* receptors.

To assess the involvement of NDUFS4-Ser173 phosphorylation in mtCB₁-dependent effects, we generated a phosphomimetic mutant of NDUFS4 in which the Ser173 residue was replaced by a Glu residue (NDUFS4-PM) (Fig. 2f, Extended Data Fig. 3f). Expression of NDUFS4-PM in cultured astrocytes abolished the decrease in NDUFS1 levels and complex I activity that was induced by THC or HU210, without affecting the activity of citrate synthase (Fig. 2g, h, Extended Data Fig. 3g, h). We then stereotactically injected a viral vector that expresses NDUFS4-PM under the control of the human *GFAP* promoter (AAV-gfa-ABC₁D-NDUFS4-PM-IRES-mRuby; here called AAV-GFAP-NDUFS4-PM)²⁵ in both the

hippocampus and the PFC of wild-type mice. The astroglial expression of NDUFS4-PM in both brain regions (Extended Data Fig. 4) totally blocked the selective degradation of the N-module of complex I and its activity induced by intraperitoneal injection of THC (Fig. 2i, Extended Data Fig. 3i). Thus, cannabinoids destabilize astroglial complex I by decreasing the phosphorylation of NDUFS4 in a mtCB₁-dependent manner.

MtCB₁ regulates astroglial mROS

The complex I N-module, which is specifically destabilized by mtCB₁ activation, contains a binding pocket for O₂ molecules that accepts electrons from NADH(H⁺) to generate mROS²³. Notably, a 24-h incubation with THC or HU210 decreased the production of mROS in astrocytes from wild-type mice but not from CB₁-KO mice (Fig. 3a, Extended Data Fig. 5a, b) in a manner that depended on the presence of intracellular CB₁ and mtCB₁ (Fig. 3b, c). Expression of NDUFS4-PM in astrocytes did not alter the levels of mROS per se (Extended Data 5c), but it abolished the decrease in mROS that was induced by THC or HU210 (Fig. 3d). Fluorescence-activated cell sorting (FACS) analysis (Extended Data Fig. 5d) of GFAP-positive cells acutely isolated from the hippocampus and PFC (Extended Data Fig. 5e) revealed that a similar reduction of mROS was induced 24 h after THC treatment (Fig. 3e). Viral intravenous administration²⁶ of a plasmid to express the NDUFS4-PM mutant in a large number of astrocytes did not significantly alter mROS levels in the hippocampus and PFC (Extended Data Fig. 5f), but it abolished the effect of THC (Fig. 3f). Thus, the cannabinoid-induced reduction of astroglial mROS is due to destabilization of the N-module of complex I through reduced phosphorylation of NDUFS4-Ser173.

Effects of MtCB₁ on glycolysis and lactate

In resting conditions, astrocytes produce higher amounts of mROS than do neurons⁹. The transcription factor hypoxia-inducible factor 1 (HIF-1) is known to sense mROS and to adapt the cell metabolism accordingly^{27–30}. Treatment with THC or HU210 decreased, in a CB₁-dependent manner, the nuclear levels of the HIF-1 regulatory subunit HIF-1 α , as well as the promoter activity of HIF-1 and the expression of HIF-1 target genes in cultured mouse astrocytes (Fig. 3g, Extended Data Fig. 6a–c). Similarly, THC decreased the expression of HIF-1 α in both the hippocampus and the PFC of GFAP-CB₁-WT mice, but not GFAP-CB₁-KO littermates (Fig. 3h, Extended Data Fig. 6d). Astroglial expression of NDUFS4-PM abolished the THC-induced decrease of HIF-1 α both in culture (Fig. 3i, Extended Data 6e) and in hippocampus and PFC samples from THC-treated mice (Fig. 3j, Extended Data Fig. 6f). Thus, the mtCB₁-dependent decrease in NDUFS4-Ser173 phosphorylation, the destabilization of the N-module of complex I and the reduced generation of mROS eventually lead to the downregulation of the HIF-1 pathway in astrocytes.

The HIF-1 pathway stimulates glycolysis in cells³¹. Incubation of cultured mouse astrocytes with THC or HU210 for 24 h decreased the release of lactate—which typically reflects glycolytic activity³²—in a dose- and CB₁-dependent way (Fig. 4a, b). THC or HU210 treatment strongly decreased the rate of glycolysis³³ in cultured astrocytes in a mtCB₁-dependent manner (Fig. 4c, d). Expression of NDUFS4-PM, which restored the cannabinoid-mediated reduction of HIF-1, abolished the THC- or HU210-induced decrease of lactate release (Fig. 4e). In addition, overexpression of HIF-1 α (Extended Data Fig. 6g, h) blunted the THC- or HU210-induced decrease of lactate release (Fig. 4f). Together, these results indicate that downregulation of the HIF-1 pathway is responsible for the decreased glycolytic activity and lactate release induced by activation of mtCB₁ in astrocytes.

Lactate that is produced by astrocytes is a key energetic support to sustain neuronal activity and functions^{1,34}. Drug-naïve neurons co-cultured for 24 h with astrocytes that were previously treated with

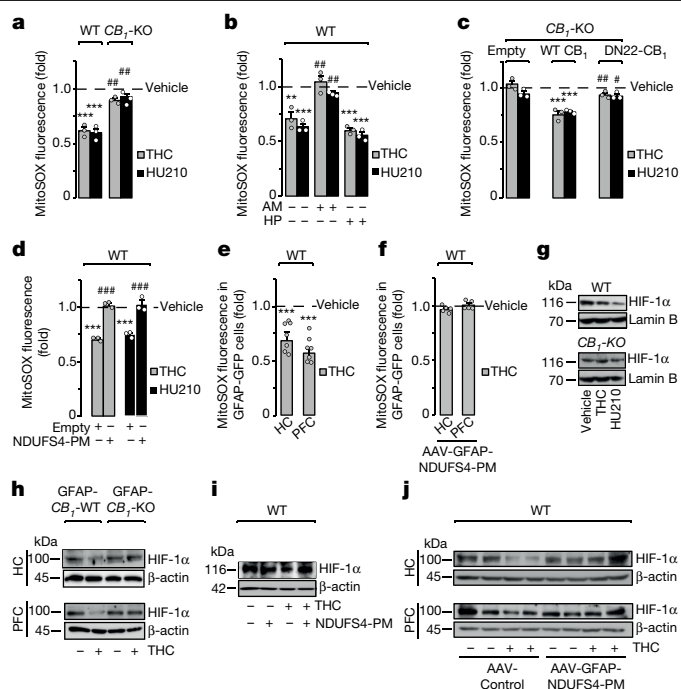


Fig. 3 | MtCB₁-dependent destabilization of complex I reduces levels of mROS and leads to downregulation of the astroglial HIF-1 pathway. **a**, Effects of THC (1 μ M) or HU210 (50 nM) treatment on mROS levels (detected using the fluorescent probe MitoSOX) in wild-type and CB₁-KO astrocytes ($n = 3$). P values by two-way ANOVA; *** $P < 0.001$ (versus vehicle); ## $P < 0.01$ (versus wild type). **b**, Effects of AM251 (1 μ M) or haemopressin (10 μ M) treatment on the cannabinoid-induced decrease in mROS in wild-type astrocytes ($n = 3$). P values by one-way ANOVA; ** $P < 0.01$, *** $P < 0.001$ (versus vehicle); ## $P < 0.01$ (versus cannabinoid agonist). **c**, Effects of THC or HU210 treatment on mROS levels in CB₁-KO astrocytes that were transfected with empty vector or that express wild-type CB₁ or DN22-CB₁ ($n = 3$). P values by two-way ANOVA; *** $P < 0.001$ (versus vehicle); * $P < 0.05$, ## $P < 0.01$ (versus wild-type CB₁). **d**, Effects of NDUFS4-PM expression on the cannabinoid-induced decrease of mROS in wild-type astrocytes ($n = 3$). P values by one-way ANOVA; *** $P < 0.001$ (versus vehicle); ### $P < 0.001$ (versus cannabinoid agonist). **e**, Effects of THC treatment (10 mg kg⁻¹) on mROS levels in astrocytes from the hippocampus and PFC ($n = 7$). P values by two-sided t -test; *** $P < 0.001$ (versus vehicle). **f**, Effects of viral expression of NDUFS4-PM by retro-orbital injection on the THC-mediated decrease in mROS in astrocytes from the hippocampus and PFC ($n = 5$). **g**, Effects of THC (1 μ M) or HU210 (50 nM) treatment on the nuclear levels of HIF-1 α in wild-type and CB₁-KO astrocytes. **h**, Effects of THC treatment (10 mg kg⁻¹) on the levels of HIF-1 α in the hippocampus or PFC of GFAP-CB₁-WT and GFAP-CB₁-KO mice. **i**, Effects of astroglial expression of NDUFS4-PM on the THC-induced decrease of HIF-1 α in astrocytes. **j**, Effects of astroglial expression of NDUFS4-PM on the THC-induced decrease of HIF-1 α in the hippocampus or PFC. In **a–f**, data are mean \pm s.e.m. and n represents the number of independent experiments. Lamin B (**g**) and β -actin (**h–j**) were used as loading controls. For original gels, see Supplementary Fig. 1; for statistical details, see Supplementary Table 1.

THC or HU210 showed intracellular neuronal bioenergetic and redox stress, as judged by a decrease in mitochondrial membrane potential ($\Delta\psi_m$) (Extended Data Fig. 7a, b) and an increase in mROS generation (Fig. 4g). Supplementing these co-cultures with lactate protected neurons against cannabinoid-induced stress (Fig. 4h, Extended Data Fig. 7c). FACS analyses (Extended Data Figs. 5d, 7d) revealed that intraperitoneal injection of THC increased the levels of mROS and apoptosis in freshly isolated neurons from the hippocampus and PFC of wild-type mice 24 h after treatment (Fig. 4i, Extended Data Fig. 7e). These effects were rescued by intracerebroventricular (ICV) supplementation of lactate (Fig. 4i, Extended Data Fig. 7e) or by viral expression of NDUFS4-PM in astrocytes (Fig. 4j, Extended Data Fig. 7f–h). Thus, the functional

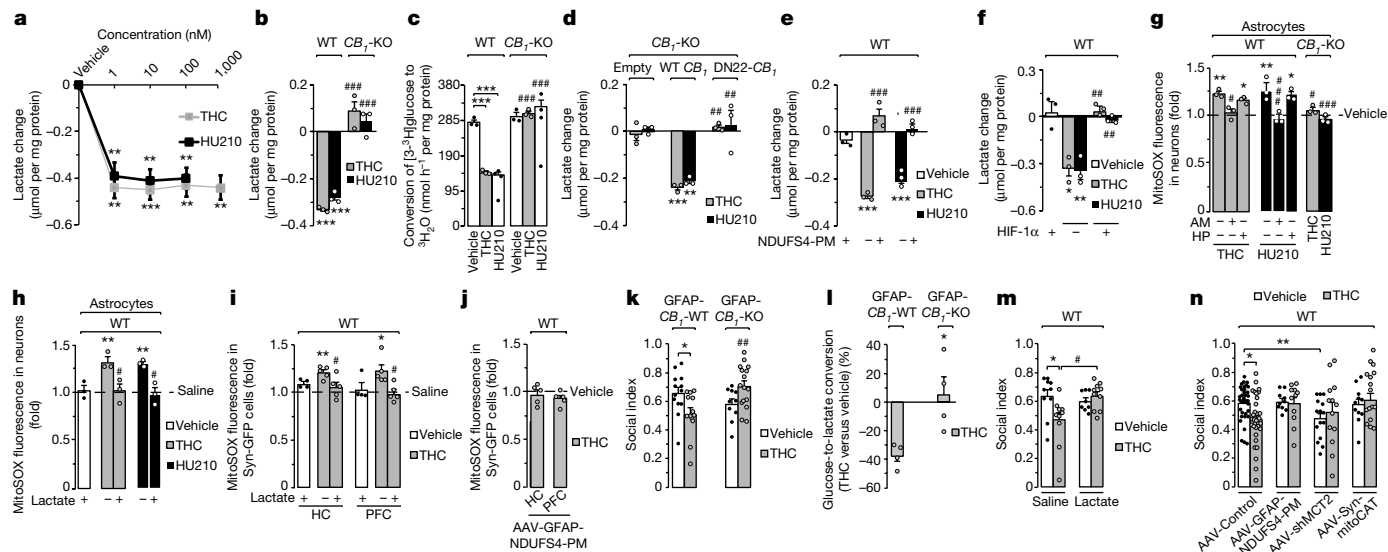


Fig. 4 | Astroglial mtCB₁ activation decreases the production of lactate and mediates the THC-induced impairment of social behaviour. **a**, Change in the production of lactate in cultured wild-type astrocytes after treatment with THC (1 μM) or HU210 (50 nM) (*n* = 3). ***P* < 0.01, ****P* < 0.001 (versus vehicle). **b, c**, Effects of THC or HU210 treatment on lactate production (**b**) and glycolysis (**c**) in wild-type and CB₁-KO astrocytes (*n* = 3). ****P* < 0.001 (versus vehicle); ###*P* < 0.001 (versus wild type). **d**, Change in the production of lactate in CB₁-KO astrocytes that were transfected with empty vector or that express wild-type CB₁ or DN22-CB₁ after treatment with THC or HU210 (*n* = 3). ***P* < 0.01, ****P* < 0.001 (versus vehicle); ###*P* < 0.01 (versus wild-type CB₁). **e, f**, Effects of overexpression of NDUFS4-PM (**e**) or HIF-1α (**f**) on the cannabinoid-induced decrease in lactate release (*n* = 3). **P* < 0.05, ***P* < 0.01, ****P* < 0.001 (versus vehicle); #*P* < 0.01, ###*P* < 0.001 (versus empty vector). **g**, Effects of THC or HU210 treatment on mROS levels in neurons that were co-cultured with wild-type or CB₁-KO astrocytes (*n* = 3). **P* < 0.05, ***P* < 0.01 (versus vehicle); #*P* < 0.05, ###*P* < 0.001 (versus cannabinoid). **h**, Effects of lactate supplementation (2 mM) on mROS levels in neurons that were co-cultured with astrocytes pretreated with THC or HU210 (*n* = 3). ***P* < 0.01 (versus saline);

#*P* < 0.05; (versus cannabinoid). **i**, Effects of ICV infusion of lactate (100 mM) on THC-induced increase in mROS in neurons from the hippocampus or PFC (*n* = 5). **P* < 0.05, ***P* < 0.01 (versus saline); #*P* < 0.001 (versus cannabinoid). **j**, Effects of viral expression of NDUFS4-PM by retro-orbital injection on the THC-induced increase in mROS in neurons from the hippocampus or PFC (*n* = 5). **k, l**, Effects of THC treatment (10 mg/kg) on social interaction (**k**) and brain glucose-to-lactate conversion (**l**) in GFAP-CB₁-KO and GFAP-CB₁-WT mice (**k**, GFAP-CB₁-KO vehicle, *n* = 10; GFAP-CB₁-KO THC, *n* = 16; GFAP-CB₁-WT, *n* = 16; **l**, *n* = 4). **P* < 0.05 (versus vehicle or GFAP-CB₁-WT); #*P* < 0.01 (versus wild-type THC). **m**, ICV infusion of lactate blocks THC-induced social impairment (for *n* numbers, see Extended Data Fig. 9). **P* < 0.05 (versus vehicle); #*P* < 0.05 (versus THC saline). **n**, Effects of THC on social interaction in mice that were stereotactically infused with AAV-control, AAV-GFAP-NDUFS4-PM, AAV-shMCT2 or AAV-Syn-MitoCAT (for *n* numbers, see Extended Data Fig. 9). **P* < 0.05; ***P* < 0.01 (versus AAV-control). All data are mean ± s.e.m.; *n* represents the number of independent experiments in **a–j** and the number of mice in **k–n**. *P* values by one-way ANOVA (**a**), two-way ANOVA (**b–k, m, n**) or unpaired two-sided *t*-test (**l**). For statistical details, see Supplementary Table 1.

viability of neurons is affected by the mtCB₁-induced downregulation of the HIF-1 pathway and the consequent reduction of glycolytic activity and lactate release in neighbouring astrocytes.

Astroglial mtCB₁ and social behaviours

To investigate the potential effects of these molecular mechanisms on mouse behaviour, we first tested whether typical short-term behavioural effects of cannabinoids persisted over 24 h after intraperitoneal injection of THC (10 mg per kg body weight). The drug had no persistent effect on prepulse inhibition of startle responses (PPI), locomotion or anxiety-like behaviour (Extended Data Fig. 8a–d), but it led to impairments in spontaneous alternation and social interaction (Fig. 4k, Extended Data Fig. 8e–g, Supplementary Videos 1–10). Notably, only the social interaction deficit was abolished in GFAP-CB₁-KO mice (Fig. 4k, Extended Data Fig. 8e–g). Whereas the rate of conversion of glucose to lactate in the brain did not differ between GFAP-CB₁-WT and GFAP-CB₁-KO littermates (GFAP-CB₁-WT, 50.7 ± 7.2%; GFAP-CB₁-KO mice, 53.1 ± 7.8% (mean ± s.e.m); *P* > 0.9), intraperitoneal injection of THC reduced this value in GFAP-CB₁-WT mice but not in GFAP-CB₁-KO littermates (Fig. 4l, Extended Data Fig. 8h), indicating that cannabinoids decrease lactate conversion via astroglial CB₁. Notably, ICV injection of lactate⁴ abolished the THC-induced social interaction impairments without exerting any significant effect per se on the social behaviour of control mice (Fig. 4m, Extended Data Fig. 9a–e). Astroglial expression of NDUFS4-PM (Extended Data Fig. 4) in the hippocampus and PFC

abolished the THC-induced impairment of social interactions (Fig. 4n, Extended Data Fig. 9f–h). These data suggest that the same mechanisms that lead to reduced lactate supply and the metabolic effects that we observed also underlie THC-induced social effects.

Downstream effects of lactate decrease

In addition to its metabolic roles, lactate can act through the specific G-protein-coupled receptor GPR81 (ref. ³⁵). The ICV infusion of two saturating doses of the GPR81 agonist 3,5-dihydroxybenzoic acid (DHBA)³⁶ before the sociability test did not block the effect of THC on social interactions (Extended Data Fig. 9i–k), which probably excludes the involvement of these receptors. Metabolically, lactate shuttles from astrocytes to neurons through monocarboxylate transporters (MCTs), predominantly neuronal MCT2 (ref. ³⁷). To further investigate the role of lactate in THC-induced impaired social behaviour, we virally expressed a short hairpin RNA (shRNA) that reduces the expression of MCT2 (ref. ³⁸) in the hippocampus and PFC. Decreased MCT2 expression resulted in a decrease in social interactions and thereby occluded the THC effect (Fig. 4n, Extended Data Fig. 9f–h), reinforcing the role of lactate shuttling between astrocytes and neurons in this behaviour.

Next, we investigated whether relieving the astroglial mtCB₁-dependent neuronal bioenergetic stress might compensate for the social effects induced by THC. Local injection of a viral vector that induces the neuronal expression of a mitochondrial form of the ROS scavenger enzyme catalase²⁶ (AAV-Syn-mitoCAT) into the hippocampus

and PFC did not alter social interactions per se, but it abolished the THC-induced impairment (Fig. 4n, Extended Data Figs. 9f–h, 10). Together, these data indicate that excessive mROS production in neurons, induced by an astroglial mtCB₁-dependent decrease of lactate, mediates the cannabinoid-induced impairment of social interactions.

Our data reveal that mitochondrial G-protein-coupled receptors can affect the bioenergetics of specific cell types and determine intercellular metabolic interactions, thereby regulating animal behaviour. Specifically, we show that mtCB₁ regulates astroglial glycolysis and lactate production through a precise molecular cascade to eventually govern the metabolic state of neurons and control social interactions (Extended Data Fig. 11). Metabolic processes are thus markedly different between astrocytes and neurons^{9,26} and they do not merely affect steady-state bioenergetics of the brain, but also have a key signalling function to regulate behavioural responses.

Therefore, the apparently obvious statement that brain metabolism is fundamental for the regulation of behavioural functions actually hides high levels of complexity, owing to the fine heterogeneity of different mechanisms that the brain uses to transform energy^{39,40}. This work establishes a cell-type-specific mechanistic framework that will have to be taken into account in studies of the pharmacological and pathophysiological functions of the endocannabinoid system and of the bioenergetic brain processes that regulate animal behaviour.

Online content

Any methods, additional references, Nature Research reporting summaries, source data, extended data, supplementary information, acknowledgements, peer review information; details of author contributions and competing interests; and statements of data and code availability are available at <https://doi.org/10.1038/s41586-020-2470-y>.

- Magistretti, P. J. & Allaman, I. Lactate in the brain: from metabolic end-product to signalling molecule. *Nat. Rev. Neurosci.* **19**, 235–249 (2018).
- Barros, L. F. & Weber, B. CrossTalk proposal: an important astrocyte-to-neuron lactate shuttle couples neuronal activity to glucose utilisation in the brain. *J. Physiol.* **596**, 347–350 (2018).
- Bolaños, J. P. Bioenergetics and redox adaptations of astrocytes to neuronal activity. *J. Neurochem.* **139**, 115–125 (2016).
- Suzuki, A. et al. Astrocyte-neuron lactate transport is required for long-term memory formation. *Cell* **144**, 810–823 (2011).
- Allen, N. J. & Barres, B. A. Glia — more than just brain glue. *Nature* **457**, 675–677 (2009).
- Hansson, E. & Rönnbäck, L. Astrocytes in neurotransmission. a review. *Cell. Mol. Biol.* **36**, 487–496 (1990).
- Araque, A. et al. Gliotransmitters travel in time and space. *Neuron* **81**, 728–739 (2014).
- Almeida, A., Almeida, J., Bolaños, J. P. & Moncada, S. Different responses of astrocytes and neurons to nitric oxide: the role of glycolytically generated ATP in astrocyte protection. *Proc. Natl Acad. Sci. USA* **98**, 15294–15299 (2001).
- Lopez-Fabuel, I. et al. Complex I assembly into supercomplexes determines differential mitochondrial ROS production in neurons and astrocytes. *Proc. Natl Acad. Sci. USA* **113**, 13063–13068 (2016).
- Semenza, G. L., Roth, P. H., Fang, H. M. & Wang, G. L. Transcriptional regulation of genes encoding glycolytic enzymes by hypoxia-inducible factor 1. *J. Biol. Chem.* **269**, 23757–23763 (1994).
- Busquets-García, A., Bains, J. & Marsicano, G. CB₁ receptor signaling in the brain: extracting specificity from ubiquity. *Neuropsychopharmacology* **43**, 4–20 (2018).
- Araque, A., Castillo, P. E., Manzoni, O. J. & Tonini, R. Synaptic functions of endocannabinoid signaling in health and disease. *Neuropharmacology* **124**, 13–24 (2017).
- Robin, L. M. et al. Astroglial CB₁ receptors determine synaptic D-serine availability to enable recognition memory. *Neuron* **98**, 935–944 (2018).

- Bénard, G. et al. Mitochondrial CB₁ receptors regulate neuronal energy metabolism. *Nat. Neurosci.* **15**, 558–564 (2012).
- Hebert-Chatelain, E. et al. A cannabinoid link between mitochondria and memory. *Nature* **539**, 555–559 (2016).
- Mendizabal-Zubiaga, J. et al. Cannabinoid CB₁ receptors are localized in striated muscle mitochondria and regulate mitochondrial respiration. *Front. Physiol.* **7**, 476 (2016).
- Aquila, S. et al. Human sperm anatomy: ultrastructural localization of the cannabinoid1 receptor and a potential role of anandamide in sperm survival and acrosome reaction. *Anat. Rec.* **293**, 298–309 (2010).
- Koch, M. et al. Hypothalamic POMC neurons promote cannabinoid-induced feeding. *Nature* **519**, 45–50 (2015).
- Gutiérrez-Rodríguez, A. et al. Localization of the cannabinoid type-1 receptor in subcellular astrocyte compartments of mutant mouse hippocampus. *Glia* **66**, 1417–1431 (2018).
- Hebert-Chatelain, E. et al. Cannabinoid control of brain bioenergetics: exploring the subcellular localization of the CB₁ receptor. *Mol. Metab.* **3**, 495–504 (2014).
- Han, J. et al. Acute cannabinoids impair working memory through astroglial CB₁ receptor modulation of hippocampal LTD. *Cell* **148**, 1039–1050 (2012).
- Guaras, A. M. & Enríquez, J. A. Building a beautiful beast: mammalian respiratory complex I. *Cell Metab.* **25**, 4–5 (2017).
- Mimaki, M., Wang, X., McKenzie, M., Thorburn, D. R. & Ryan, M. T. Understanding mitochondrial complex I assembly in health and disease. *Biochim. Biophys. Acta* **1817**, 851–862 (2012).
- De Rasmio, D., Panelli, D., Sardanelli, A. M. & Papa, S. cAMP-dependent protein kinase regulates the mitochondrial import of the nuclear encoded NDUFS4 subunit of complex I. *Cell Signal.* **20**, 989–997 (2008).
- Hammond, S. L., Leek, A. N., Richman, E. H. & Tjalkens, R. B. Cellular selectivity of AAV serotypes for gene delivery in neurons and astrocytes by neonatal intracerebroventricular injection. *PLoS ONE* **12**, e0188830 (2017).
- Vicente-Gutierrez, C. et al. Astrocytic mitochondrial ROS modulate brain metabolism and mouse behavior. *Nat. Metab.* **1**, 201–211 (2019).
- Chandel, N. S. et al. Mitochondrial reactive oxygen species trigger hypoxia-induced transcription. *Proc. Natl Acad. Sci. USA* **95**, 11715–11720 (1998).
- Patten, D. A. et al. Hypoxia-inducible factor-1 activation in nonhypoxic conditions: the essential role of mitochondrial-derived reactive oxygen species. *Mol. Biol. Cell* **21**, 3247–3257 (2010).
- Shadel, G. S. & Horvath, T. L. Mitochondrial ROS signaling in organismal homeostasis. *Cell* **163**, 560–569 (2015).
- Semenza, G. L. Hypoxia-inducible factors: coupling glucose metabolism and redox regulation with induction of the breast cancer stem cell phenotype. *EMBO J.* **36**, 252–259 (2017).
- Semenza, G. L. Dynamic regulation of stem cell specification and maintenance by hypoxia-inducible factors. *Mol. Aspects Med.* **47–48**, 15–23 (2016).
- Almeida, A., Moncada, S. & Bolaños, J. P. Nitric oxide switches on glycolysis through the AMP protein kinase and 6-phosphofructo-2-kinase pathway. *Nat. Cell Biol.* **6**, 45–51 (2004).
- Herrero-Mendez, A. et al. The bioenergetic and antioxidant status of neurons is controlled by continuous degradation of a key glycolytic enzyme by APC/C-Cdh1. *Nat. Cell Biol.* **11**, 747–752 (2009).
- Jimenez-Blasco, D., Santofimia-Castaño, P., Gonzalez, A., Almeida, A. & Bolaños, J. P. Astrocyte NMDA receptors' activity sustains neuronal survival through a Cdk5–Nrf2 pathway. *Cell Death Differ.* **22**, 1877–1889 (2015).
- Morland, C. et al. The lactate receptor, G-protein-coupled receptor 81/hydroxycarboxylic acid receptor 1: expression and action in brain. *J. Neurosci. Res.* **93**, 1045–1055 (2015).
- Liu, C. et al. 3,5-Dihydroxybenzoic acid, a specific agonist for hydroxycarboxylic acid 1, inhibits lipolysis in adipocytes. *J. Pharmacol. Exp. Ther.* **341**, 794–801 (2012).
- Pierre, K., Magistretti, P. J. & Pellerin, L. MCT2 is a major neuronal monocarboxylate transporter in the adult mouse brain. *J. Cereb. Blood Flow Metab.* **22**, 586–595 (2002).
- Mazuel, L. et al. A neuronal MCT2 knockdown in the rat somatosensory cortex reduces both the NMR lactate signal and the BOLD response during whisker stimulation. *PLoS One* **12**, e0174990 (2017).
- Hollis, F. et al. Mitochondrial function in the brain links anxiety with social subordination. *Proc. Natl Acad. Sci. USA* **112**, 15486–15491 (2015).
- Picard, M., McEwen, B. S., Epel, E. S. & Sandi, C. An energetic view of stress: focus on mitochondria. *Front. Neuroendocrinol.* **49**, 72–85 (2018).

Publisher's note Springer Nature remains neutral with regard to jurisdictional claims in published maps and institutional affiliations.

© The Author(s), under exclusive licence to Springer Nature Limited 2020

Methods

Mice

All experimental procedures were approved by the Committee on Animal Health and Care of INSERM and the French Ministry of Agriculture and Forestry (authorization numbers, A501350, A3310035, C33063096) and by the Bioethics Committee of the University of Salamanca in accordance with the Spanish legislation (RD53/2013). Male C57BL/6-N mice purchased from Janvier or bred in the University of Salamanca, *CB₁*-KO male mice bred at the Complutense University of Madrid and male inducible GFAP-*CB₁*-KO mutant mice and their wild-type (GFAP-*CB₁*-WT) littermates²¹ bred at the Neurocentre Magendie were used in this study. As previously shown, to obtain the deletion of the astroglial CB₁ receptor, tamoxifen was daily injected (1 mg/kg, intraperitoneally (i.p.)) for 8 days. Three weeks after the last injection of tamoxifen we performed the *in vivo* experiments in both GFAP-*CB₁*-KO and GFAP-*CB₁*-WT mice. The age of the mice at the beginning of all the behavioural experiments was 8–12 weeks. All experiments were performed during the first part of the light phase (09:00. to 14:00). Experimenters were always blinded to treatments and genotypes.

Reagents

For *in vitro* experiments sodium L-lactate (2 mM; L7022, Sigma-Aldrich) was dissolved in culture medium. THC (1–1,000 nM, THC Pharm), WIN (100 nM, Sigma-Aldrich), HU210 (1–100 nM, Tocris), HU210-biotin²⁴ (1 μM), AM251 (1 μM; ab120088, Abcam), SR141716A (1 μM; 0923, Tocris), haemopressin (5–10 μM; 3791, Tocris) and KH7 (5 μM, Sigma-Aldrich) were dissolved in dimethyl sulfoxide (DMSO; maximum final DMSO concentration was 0.1%). The doses and concentrations of the different reagents were chosen from previous published data^{14,15,20,41} or from preliminary experiments as specified in the main text and/or figure legends.

For *in vivo* administrations, sodium L-lactate (100 mM; 71718, Sigma-Aldrich) and the specific GPR81 agonist 3,5-DHBA (100 nM and 1 mM; 4599, Sigma-Aldrich) were dissolved in saline. THC (10 mg/kg, i.p.) was purchased from THC-Pharm and dissolved in 4% ethanol, 4% Cremophor-EL and 92% saline. THC was injected in a volume of 10 ml/kg.

Virus generation

AAV-gfa-ABC₁D-IRES-mRuby, AAV-hSyn-IRES-mRuby, AAV-gfa-ABC₁D-NDUFS4-PM-IRES-mRuby and AAV-hSyn-MitoCAT-IRES-mRuby viral constructs were generated using standard molecular cloning techniques described for other viral constructs used before in the laboratory^{15,25}. In brief, the coding sequence of NDUFS4-PM²⁴ and MitoCAT²⁶ were cloned into gfa-ABC₁D-GFP (Addgene plasmid #50473) or AAV-hSyn-GFP (Addgene plasmid #50465), respectively. The GFP sequence inside the vector was replaced by NDUFS4-PM or MitoCAT coupled to the IRES-mRuby sequence for correct visualization of transfected cells. Viral particles (AAV8 serotype) were produced by polyethylenimine transfection of HEK293T cells (obtained from ATCC, CRL-3216, lot number #62729596) and subsequent iodixanol density gradient purification as previously described^{15,25}. The AAV2/DJ-CBA-mCherry-miR30E-shMCT2⁴² was provided by L. Pellerin.

Cell cultures and co-cultures

Primary cultures of brain cortical neurons were prepared from C57BL/6 mice of 15.5 days of gestation. Cell suspensions were seeded at 2.5×10^5 cells/cm² in different size plastic plates previously coated with poly-D-lysine (10 μg/ml) and incubated in Neurobasal A (Life Technologies) supplemented with 5.5 mM of glucose, 2 mM of glutamine, 0.25 mM of pyruvate and 2% MAO (Minus Antioxidant) B27 supplement (Life Technologies). Cells were incubated at 37 °C in a humidified 5% CO₂-containing atmosphere. At 72 h after plating, the medium was

replaced and the neurons were used for the experiments on day 7 *in vitro* (DIV).

Primary cultures of brain cortical astrocytes were prepared from either C57BL/6 wild-type or *CB₁*-KO⁴³ neonatal mice of 0–1 days old. Cell suspensions were seeded at 2.5×10^5 cells in 175-cm² plastic flasks and incubated in Dulbecco's modified Eagle's medium (DMEM) supplemented with 10% fetal bovine serum (FBS). Non-astroglial cells were detached after 7 DIV by shaking the flasks at 200 rpm overnight and discarding the supernatant. The remaining attached, astrocyte-enriched cells were re-seeded in different size plastic plates and further incubated for 7 DIV for the experiments.

For the astrocyte–neuron co-cultures, astrocytes were re-seeded on inserts (0.4-μm pore size, Millipore Merck) and incubated for 5 DIV in DMEM containing 10% FBS. Then, cells were washed with phosphate-buffered saline (PBS, pH 7.4) and further incubated for 24 h in Neurobasal A containing glucose (5.5 mM), glutamine (2 mM), pyruvate (0.25 mM) and MAO-B27 supplement (2%), either in the absence or in the presence of THC (1 μM) or HU210 (50 nM). After this period, inserts containing the cells were thoroughly washed with PBS, placed on the top of 6 DIV neuronal culture and incubated for 24 h in Neurobasal A containing glucose (5.5 mM), glutamine (2 mM), pyruvate (0.25 mM) and MAO-B27 supplement (2%) in the absence of THC or HU210.

Plasmid construction and site-directed mutagenesis

The N-terminal deletion of the first 22 amino acids (66 base pairs) in the mouse CB₁ receptor coding sequence to obtain the DN22-CB₁ mutant was achieved by polymerase chain reaction (PCR). In brief, for DN22-CB₁ a forward primer hybridizing from the 67th base starting from ATG was coupled to a reverse primer hybridizing to the end of the coding sequence, including the TGA stop codon. To guarantee proper translation of the construct, the forward primer included an ATG codon upstream of the hybridizing sequence. The cDNA for DN22-CB₁ (ref. ¹⁵) was amplified using HF Platinum DNA polymerase (Invitrogen) and inserted into a PCRII-Topo vector (Invitrogen) according to the manufacturer's instructions. The absence of amplification mismatches was then verified by DNA sequencing. The primers used were: forward 5'-**ATGGTGGGCTCAAATGACATTCAG**-3' (in bold the inserted ATG), reverse 5'-**TCACAGAGCCTCGGCAGACGTG**-3' (stop codon in bold). The cDNA sequence for CB₁ or DN22-CB₁ was inserted into a modified version of the pcDNA3.1 mammalian expression vector using BamHI-EcoRV according to standard cloning procedures. CB₁ or DN22-CB₁ was fused to GFP by using the pEGFP-N1 vector (Addgene) according to the manufacturer's instructions for control of transfection efficiency.

The phosphomimetic version of NDUFS4 was synthesized from the full-length human NDUFS4 sequence (provided by S. Papa)²⁴. The NDUFS4 cDNA constructs were engineered to contain 5' HindIII and 3' XhoI and cloned in a pcDNA3.1(+) vector with the T7 promoter. cDNA constructs were then subjected to site-directed mutagenesis on Ser173 (the phosphorylation site of PKA), which was replaced by a glutamic acid residue to obtain the Ser173Glu phosphomimetic version of NDUFS4 (NDUFS4-PM) using the QuikChange XL kit (Stratagene), followed by DpnI digestion. The forward and reverse oligonucleotides designed for this mutation were, 5'-GGAACAAAAGAACAAGAGTAGAAACAAAATAG-3' and 5'-CTATTTGTTTCTACTCTTGTCTTTTGTCC-3' (the Glu codon is indicated in bold).

The full-length cDNA encoding human HIF-1α was a gift from S. Cadenas.

Cell transfections and treatments

All cell transfections with plasmids were performed using Lipofectamine LTX + Reagent Plus (Invitrogen) following the manufacturer's instructions. Astrocytes were transfected with 0.16–1.6 μg/ml of the plasmids and, after 1 h, cells were incubated with the drugs (THC, HU210, AM251, SR141716A or haemopressin) for another 24 h.

Subcellular fractionation

To fractionate cytosol from nucleus, cells were washed with cold PBS containing 1 mM MgCl₂, collected with cytosolic buffer (10 mM HEPES, 1.5 mM MgCl₂, 10 mM KCl, 1 mM EDTA, NP-40 0.1%, v/v, 1.5 M sucrose and protease and phosphatase inhibitors cocktail, pH 7.9), triturated with a micropipette to promote cell lysis, left on ice for 30 min and vortexed for 10 s. After checking cell lysis under a light microscope, extracts were centrifuged at 830g for 10 min and the cytosolic fraction (supernatant) was removed and boiled for 5 min. Lysis of the nuclei was performed by resuspending the nuclear pellet in nuclear buffer (50 mM HEPES, 1.5 mM MgCl₂, 10 mM KCl mM, 0.5 mM NaCl, 1 mM EDTA, NP-40 1%, v/v and protease and phosphatase inhibitor cocktail, pH 7.9), triturating with a micropipette, leaving on ice for 2 h, vortexing (10 s), boiling (5 min) and sonicating (5 min).

Blue native gel electrophoresis

To assess the mitochondrial respiratory complexes, digitonin-solubilized mitochondria (10–50 µg) were loaded in NativePAGE Novex 3–12% gels (Life Technologies, New York, USA). After electrophoresis, in-gel NADH dehydrogenase activity (IGA-BNGE) was evaluated⁹ and the individual complex I and complex I-containing supercomplex (SC) bands identified. Individual complex I or complex I-containing SC bands were excised from the gel and denatured in 1% SDS (containing 1% β-mercaptoethanol) for 1 h. The proteins contained in the gel slices were separated electrophoretically, followed by western blotting against specific antibodies. Direct transfer of BNGE was also performed, when indicated, after soaking the gels for 20 min (4 °C) in carbonate buffer (10 mM NaHCO₃, 3 mM Na₂CO₃·10H₂O, pH 9.5–10). Protein transfer to PVDF membranes was carried out at 300 mA and 60 V for 1.5 h at 4 °C in carbonate buffer.

Electron microscopy

Electron microscopy was performed following a published protocol⁴⁴. Coronal hippocampal CA1, prefrontal (prelimbic) cortex (PFC), nucleus accumbens and piriform cortex containing vibrosections of mice were cut at 50 µm and collected in 0.1 M phosphate buffer (PB) (pH 7.4) with 0.1% sodium azide at room temperature. They were transferred and preincubated in a blocking solution of 10% bovine serum albumin (BSA), 0.1% sodium azide and 0.02% saponin prepared in Tris–hydrogen chloride-buffered saline 1× (TBS), pH 7.4 for 30 min at room temperature. Then, the wild-type and *CB₁*-KO tissue sections were incubated with the primary guinea pig polyclonal anti-*CB₁* receptor antibody (2 µg/ml, #CB1-GP-Af530, Frontier Institute; RRID: AB_2571593) and rabbit polyclonal anti-A522 (EAAT1 [GLAST]) antibody (0.3 µg/ml, Ab#314, provided by N. C. Danbolt; RRID: AB_2314561) diluted in 10% BSA/TBS containing 0.1% sodium azide and 0.004% saponin on a shaker for 2 days at 4 °C. Then, the tissue was incubated after several washes in 1% BSA/TBS with the biotinylated anti-rabbit (1:200, BA-1000; RRID: AB_2313606) and the 1.4 nm gold-conjugated anti-guinea pig IgG (Fab' fragment) (1:100, Nanoprobes; goat; #2055) secondary antibodies in 1% BSA/TBS with 0.004% saponin for 3 h at room temperature, washed in 1% BSA/TBS and subsequently incubated in the avidin–biotin complex (1:50; PK-7100, Vector Labs) diluted in the washing solution for 1.5 h. After washing the sections in 1% BSA/TBS overnight at 4 °C, they were post-fixed with 1% glutaraldehyde in TBS for 10 min and washed in double-distilled water. Then, the gold particles were silver-intensified with a HQ Silver kit (Nanoprobes) for about 12 min in the dark, washed in 0.1 M PB (pH 7.4) and immediately afterwards incubated in 0.05% diaminobenzidine (DAB) and 0.01% hydrogen peroxide prepared in 0.1 M PB for 3 min. Finally, the sections were osmicated (1% osmium tetroxide, in 0.1 M PB pH 7.4) for 20 min, washed in 0.1 M PB (pH 7.4), dehydrated in graded alcohols (50–100%) to propylene oxide and plastic-embedded in Epon resin 812. Fifty-nanometre ultrathin sections were cut with a diamond knife (Diatome USA), collected on nickel mesh grids, stained

with 2.5% lead citrate and examined with a JEOL JEM 1400 Plus electron microscope. Tissue preparations were photographed using a digital camera coupled to the electron microscope. Minor adjustments in contrast and brightness were made to the figures using Adobe Photoshop (Adobe Systems).

Semi-quantification of the *CB₁* receptor immunogold and immunoperoxidase staining. The pre-embedding immunogold and immunoperoxidase methods were simultaneously applied and repeated three times on the sections obtained from each of the three individual wild-type and *CB₁*-KO mice studied⁴⁴. Immunogold-labelled resin-embedded sections were first visualized under the light microscope to select portions with good and reproducible *CB₁* receptor immunolabelling.

Then, three to four semi-thin sections (1-µm thick) were cut with a histo diamond knife (Diatome USA) and stained with 1% toluidine blue. To further standardize the conditions, only the first 20 ultrathin sections (50-nm thick) were cut and collected onto the grids. We randomly took 4 × 4 assemblies of 16 electron micrographs (×8,000) from each brain region (1,000 µm²), of the wild-type and *CB₁*-KO mice. Sampling was always carefully and accurately carried out in the same way for all the mice studied and experimenters were blinded to the samples during *CB₁* receptor quantification.

Positive EAAT1 (GLAST) astrocytic processes were identified by the presence of DAB immunodeposits. Positive *CB₁* receptor labelling was considered if at least one immunoparticle was within around 30 nm from the outer mitochondrial membranes. Furthermore, only particles on mitochondrial membrane segments far away from other astrocytic membranes (distance ≥ 80 nm) and well distinct from the astrocytic intermediate filaments or any other intracellular organelle membranes were considered^{20,44}. *CB₁* receptor particles per area of astrocytic or neuronal mitochondria were counted in wild-type and *CB₁*-KO mice. A one-way ANOVA was used for comparisons between cell types and *t*-test analysis was used to compare genotypes.

Immunoblotting

Primary antibodies for western blotting. Immunoblotting was performed using mouse monoclonal anti-lamin B (1:100) (sc374015, Santa Cruz Biotechnologies), mouse monoclonal anti-β-actin (1:30,000) (A5441, Sigma-Aldrich), rabbit polyclonal anti-Hsp60 (1:1,000) (ab46798, Abcam), mouse monoclonal anti-β-ATP (1:1,000) (MS503, MitoSciences), mouse monoclonal anti-HIF-1α (MAB1536, R&D Systems), mouse monoclonal anti-complex I immunocapture (1:500) (ab109798, Abcam), rabbit polyclonal anti phospho-(Ser/Thr) PKA substrate (1:1,000) (9621, Cell Signalling), goat polyclonal anti-NDUFS1 (1:500) (sc-50132, Santa Cruz Biotechnology), rabbit monoclonal anti-NDUFV2 (1:1,000) (ab183715, Abcam), mouse monoclonal anti-NDUFA9 (1:1,000) (ab14713, Abcam), mouse monoclonal anti-NDUFS2 (1:800) (ab110249, Abcam), mouse monoclonal anti-NDUF8 (1:500) (ab110242, Abcam), rabbit polyclonal anti-phospho-Ser173 NDUFS4 (1:100) (provided by D. De Rasmio)⁴⁵ and mouse monoclonal NDUFS4 (1:800) (ab87399, Abcam).

Secondary antibodies for western blotting. Immunoblotting was performed using horseradish peroxidase-conjugated goat anti-rabbit IgG, goat anti-mouse IgG or rabbit anti-goat IgG (1:10,000; Santa Cruz Biotechnologies).

Determination of protein concentrations

Protein concentrations were determined in the cell suspensions, lysates or in parallel cell culture incubations after solubilization with 0.1 M NaOH. Protein concentrations were determined with the BCA protein assay kit (Pierce) following the manufacturer's instructions, using BSA as standard.

Western blotting. Cells and subcellular fractions or brain tissues (prefrontal cortex and hippocampus) from GFAP-*CB₁*-WT and GFAP-*CB₁*-KO

were lysed in RIPA buffer (2% sodium dodecylsulfate, 2 mM EDTA, 2 mM EGTA and 50 mM Tris pH 7.5), supplemented with protease and phosphatase inhibitor cocktail (100 μ M phenylmethylsulfonyl fluoride, 50 μ g/ml antipain, 50 μ g/ml pepstatin, 50 μ g/ml amastatin, 50 μ g/ml leupeptin, 50 μ g/ml bestatin, 1 mM orthovanadate, 50 mM NaF and 50 μ g/ml soybean trypsin inhibitor) and boiled for 5 min. Extracts were centrifuged at 13,000g for 5 min at 4 °C, and aliquots of lysates (50 μ g protein, unless otherwise stated) were subjected to SDS-PAGE on a 8, 10 or 12% acrylamide gel (MiniProtean, Bio-Rad) including PageRuler Plus Prestained Protein Ladder (Thermo Fisher Scientific). The resolved proteins were transferred electrophoretically to nitrocellulose membranes (Hybond-ECL, Amersham Bioscience Europe). Membranes were blocked with 5% (w/v) low-fat milk in 20 mM Tris, 500 mM NaCl and 0.1% (w/v) Tween 20, pH 7.5, for 1 h. After blocking, membranes were immunoblotted with primary antibodies at dilutions ranging from 1:200 to 1:1,000 overnight at 4 °C. After incubation with the secondary antibodies described above (all at 1:10,000 dilution), membranes were immediately incubated with the enhanced chemiluminescence kit WesternBright ECL (Advansta) for 2 min or SuperSignal West Femto Maximum Sensitivity Substrate (Thermo Fisher Scientific) for 5 min, before exposure to Fuji Medical X-Ray film (Fujifilm), and the autoradiograms were scanned. Biologically independent replicates were always performed, and a representative western blot is shown.

Mitochondrial measurements

Mitochondria isolation and solubilization. Purified brain mitochondria were isolated as previously described from GFAP-*CB₁*-KO mice and their GFAP-*CB₁*-WT littermates^{14,15,20,41}. In brief, forebrain tissue was collected and homogenized in isolation buffer (250 mM D⁽⁺⁾-sucrose, 10 mM Tris-base (pH 7.6, HCl), 1 mM EDTA (EDTA), protease inhibitors (Roche), 10 mM Na₃VO₄, 2 mM NaF). Homogenates were centrifuged at 1,500g for 5 min. Then, the supernatant was centrifuged at 12,500g for 5 min and the pellet was kept. The cycle of centrifugation was kept, and the final pellet was added on top of a 12–7% Ficoll400 gradient for ultracentrifugation (100,000g for 1h). The obtained purified brain mitochondria were kept on ice for no more than 3 h.

Mitochondria were obtained from cell cultures according to a previously published protocol⁴⁶. In brief, cells (12 million–100 million) were collected, cell pellets frozen at –80 °C and homogenized (10 strokes) in a glass-teflon Potter-Elvehjem, in Buffer A (saccharose 83 mM; MOPS 10 mM; pH 7.2). The same volume of Buffer B (saccharose 250 mM; MOPS 30 mM) was added to the sample, and the homogenate was centrifuged (1,000g, 5 min) to remove unbroken cells and nuclei. Centrifugation of the supernatant was then performed (12,000g, 2 min) to obtain the mitochondrial fraction, which was washed in Buffer C (saccharose 320 mM; EDTA 1 mM; Tris-HCl 10 mM; pH 7.4). Mitochondria were suspended in Buffer D (6-aminohexanoic acid 1 M; Bis-Tris-HCl 50 mM; pH 7.0). Solubilization of mitochondria was performed with digitonin at 4 g/g (5 min in ice). After a 30 min centrifugation at 13,000g, the supernatant was collected.

Immunoprecipitation of complex I. For immunoprecipitation of complex I, digitonin-solubilized mitochondria (3–10 μ g) were incubated with complex I agarose-conjugated dynabeads (Life Technologies) overnight at 4 °C in an orbital roller. Proteins were eluted from the beads by heating at 70 °C for 10 min in Laemmli's buffer (5% β -mercaptoethanol, 2%; SDS, 0.05%; Bromophenol Blue, 10%; glycerol and 60 mM Tris-HCl). Eluted proteins were separated directly by SDS-PAGE (12% gel). For the input, 3 μ g of mitochondria lysates was loaded. Western blot was performed using anti-phospho-(Ser/Thr) PKA substrate, anti-NDUFS2 and anti-Hsp60 (input) antibodies.

Oxygen consumption of purified brain mitochondria and primary astrocytes. As previously described¹⁵, oxygen consumption of brain mitochondria and intact cells was measured using a Clark-type oxygen

electrode (Hansatech) at 37 °C. Purified mitochondria (75–100 μ g) were suspended in 500 μ l of respiration buffer (75 mM mannitol, 25 mM sucrose, 10 mM KCl, 10 mM Tris-HCl pH 7.4, 50 μ M EDTA). Then, pyruvate (5 mM), malate (2 mM) and ADP (5 mM) were successively added to measure complex I-dependent respiration. Drugs (THC and WIN) were directly added into the chambers. The experiments using primary cultures of brain cortical astrocytes were performed on 2×10^6 cells per ml in growth medium. Intact astrocytes were incubated with drugs (HU210, HU210-biotin, KH7) for 1 h directly in T175-cm² flasks. Astrocytes were then transferred into the chamber and basal respiration was recorded.

Detection of mROS. mROS were detected using the fluorescent probe MitoSOX (Life Technologies). Cells, astrocytes and neurons in primary culture or brain cell suspensions, were incubated, respectively, with 2 or 3 μ M of MitoSOX for 30 min at 37 °C in a 5% CO₂ atmosphere in HBSS buffer (NaCl 134.2 mM; KCl 5.26 mM; KH₂PO₄ 0.43 mM; NaHCO₃ 4.09 mM; Na₂HPO₄·2H₂O 0.33 mM; glucose 5.44 mM; HEPES 20 mM; CaCl₂·2H₂O 4 mM; pH 7.4). Cells were then washed with PBS, and the fluorescence was assessed by a FACSCalibur flow cytometer (15 mW argon ion laser tuned at 488 nm; CellQuest software, Becton Dickinson Biosciences) in arbitrary units. In all cases, antimycin A (10 μ M, Sigma-Aldrich), which increases mROS, was used as a positive control.

Assessing H₂O₂. For H₂O₂ assessments, AmplexRed (Life Technologies) was used. Cells grown on 96-well plates were washed with PBS and incubated in KRPG buffer (NaCl 145 mM; Na₂HPO₄ 5.7 mM; KCl 4.86 mM; CaCl₂ 0.54 mM; MgSO₄ 1.22 mM; glucose 5.5 mM; pH 7.35) in the presence of 9.45 μ M AmplexRed containing 0.1 U/ml of horseradish peroxidase. Luminescence was recorded for 2 h at 30-min intervals using a Varioskan Flash (Thermo Fisher Scientific) spectrofluorometer (excitation 538 nm; emission 604 nm). Slopes were used for calculations of the rates of H₂O₂ formation.

Detection of mitochondrial H₂O₂ with pHyPer-dMito by epifluorescence microscopy. The pHyPer-dMito plasmid (Evrogen) expresses a modified version of the domain OxyR from *Escherichia coli*, which is sensitive to oxidation by H₂O₂. After oxidation, a conformational change renders the protein fluorescent⁴⁷. The excitation wavelength (λ_{exc}) reaches its maximum value at 420 and 500 nm, whereas the emission wavelength (λ_{em}) stays at 516 nm. The production of H₂O₂ by mitochondria in intact cells was assessed using this approach and analysed by epifluorescence microscopy. Astrocytes grown on glass coverslips were transfected with pHyPer-dMito and, after 1 h, treated with THC or HU210 and incubated for a further 24 h. Cells were then fixed with 4% (v/v in PBS) paraformaldehyde for 20 min and incubated with DAPI (30 μ M; Sigma-Aldrich). Coverslips were washed and mounted in SlowFade light antifade reagent (Molecular Probes) on glass slides for fluorescence microphotographs at $\times 40$ magnification using a Nikon Eclipse Ti-E. The fluorescence intensities were quantified in at least five microscopic fields using the ImageJ 1.48V software.

Mitochondrial membrane potential. The mitochondrial membrane potential ($\Delta\psi_m$) was assessed using the MitoProbe DiIC₁ (1,1',3,3,3',3'-hexamethylindodicarbo-cyanine iodide, 50 nM) Assay Kit for flow cytometry (Life Technologies). For this purpose, cells, neurons in primary culture or brain cell suspensions were incubated with the dye at 37 °C for 15 min. $\Delta\psi_m$ values were expressed in arbitrary units. Cells were incubated with CCCP (carbonyl cyanide 4-(trifluoromethoxy) phenylhydrazone; 10 μ M) for 15 min and analysed to define the depolarized value ($0 \Delta\psi_m$).

Specific activity of mitochondrial respiratory complexes. Cells were collected and suspended in PBS (pH 7.0). After three cycles of freezing and thawing, to ensure cellular disruption, complex I, complex

Article

II–III, complex IV and citrate synthase activities were determined. Rotenone-sensitive complex I (NADH-ubiquinone oxidoreductase) activity⁴⁸ was measured in KH_2PO_4 (20 mM, pH 7.2) in the presence of 8 mM MgCl_2 , 2.5 mg/ml BSA, 0.15 mM NADH and 1 mM KCN. Changes in absorbance at 340 nm (30 °C) ($\epsilon = 6.81 \text{ mM}^{-1} \text{ cm}^{-1}$) were recorded after the addition of 50 μM ubiquinone and 10 μM rotenone. Complex II–III (succinate-cytochrome c oxidoreductase) activity⁴⁹ was determined in the presence of 100 mM phosphate buffer, plus 0.6 mM EDTA(K^+), 2 mM KCN and 200 μM of cytochrome c. Changes in absorbance were recorded (550 nm; 30 °C) ($\epsilon = 19.2 \text{ mM}^{-1} \text{ cm}^{-1}$) after the addition of 20 mM succinate and 10 μM antimycin A. For complex IV (cytochrome c oxidase) activity, the first rate constant (k (min^{-1} per mg protein)) of cytochrome c oxidation was determined⁵⁰ in the presence of 10 mM phosphate buffer and 50 μM of reduced cytochrome c; absorbance was recorded every minute at 550 nm, 30 °C ($\epsilon = 19.2 \text{ mM}^{-1} \text{ cm}^{-1}$). Citrate synthase activity⁵¹ was measured in the presence of 93 mM of Tris-HCl, 0.1% (v/v) triton X-100, 0.2 mM acetyl-CoA and 0.2 mM DTNB; the reaction was started with 0.2 mM of oxaloacetate and the absorbance was recorded at 412 nm (30 °C) ($\epsilon = 13.6 \text{ mM}^{-1} \text{ cm}^{-1}$).

Flow cytometric analysis of apoptotic cell death

Cells, neurons in primary culture or brain cell suspensions were stained with APC-conjugated annexin-V and 7-amino-actinomycin D (7-AAD) (Becton Dickinson Biosciences) in binding buffer (100 mM HEPES, 140 mM NaCl, 2.5 mM CaCl_2), according to the manufacturer's instructions, to determine quantitatively the percentage of apoptotic cells by flow cytometry. Cells were analysed, in three replicates per condition, on a FACSCalibur flow cytometer (15 mW argon ion laser tuned at 488 nm; CellQuest software, Becton Dickinson Biosciences). Annexin⁺ and 7-AAD⁻ cells were considered apoptotic. The analyser threshold was adjusted on the flow cytometer channel to exclude most of the subcellular debris to reduce the background noise owing to the neurite disruption during neuronal detaching. Data were expressed as fold change.

Quantitative PCR with reverse transcription analysis

This analysis was performed in total RNA samples, purified from astrocytes using a commercially available kit (Sigma-Aldrich), using the Power SYBR Green RNA-to- C_T 1-Step kit (Applied Biosystems). Reverse transcription was performed for 30 min at 48 °C, and PCR conditions were 10 min at 95 °C followed by 40 cycles of 15 s at 95 °C plus 1 min at 55 °C using the following forward and reverse primers, respectively (Thermo Fisher Scientific), 5'-TCTCAGAGCGCTCAAGACAA-3' and 5'-GATGGCACGAACCTGTAGCA-3' (*HkII*), 5'-CACCTTCTTCAAAGTCCCG-3' and 5'-ATGCTGTTCACCTCCACCG-3' (*Glut3*), 5'-GGGTGTGAACCAAGGAGAAAT-3' and 5'-GACTGTGGTCATGACCCCTT-3' (*Capdh*) and 5'-CAACGTACACTTCATGATG-3' (*Actb*). The mRNA abundance of each transcript was normalized to the β -actin mRNA abundance obtained in the same sample. The relative mRNA levels were calculated using the $\Delta\Delta\text{C}_t$ method, and were expressed as the fold change between sample and calibrator.

Rate of glycolysis and lactate concentration

The glycolytic flux was assessed as previously described³³. In brief, attached intact cells were washed with PBS and incubated in the presence of 5 $\mu\text{Ci/ml}$ of D-[3-³H]glucose in 2 ml of a Krebs–Henseleit buffer (11 mM Na_2HPO_4 , 122 mM NaCl, 3.1 mM KCl, 0.4 mM KH_2PO_4 , 1.2 mM MgSO_4 , 1.3 mM CaCl_2 ; pH 7.4) supplemented with 5.5 mM D-glucose at 37 °C with shaking in a sealed flask. Before sealing the flask with a rubber cap, a 1.5-ml Eppendorf tube containing 1 ml of water (for ³H₂O trapping) was fixed inside the flask by holding it from the flask tab using a rib, and the flask atmosphere was gassed with a O₂/CO₂ (95/5) mixture for 20 s. Flasks were incubated in the air-thermostated chamber of an orbital shaker (Forma Benchtop Orbital Shaker, Model 420, Thermo Fisher Scientific). In preliminary experiments (data not shown), we observed that ³H₂O collection in the holding tube was linear with time

for up to 120 min; therefore, all remaining incubations were performed for this period. The reactions were stopped by adding 0.2 ml of 20% v/v, HClO₄ through the rubber cap, and flasks were further incubated for 4 days to allow equilibration of ³H₂O between water and the incubation medium. In preliminary experiments using ³H₂O, we observed that the ³H₂O equilibrated between both compartments was 28% (hence reflecting an actual 70% of recovery efficiency). This efficiency value (28% for ³H₂O), was considered for the calculations. Results were expressed as nmol of D-[3-³H]glucose incorporated into ³H₂O per h and per mg protein (rate of glycolysis). Lactate concentrations were measured in the culture medium spectrophotometrically by determining the increments in absorbance of the samples at 340 nm in a mixture containing 1 mM NAD⁺ and 22.5 U/ml lactate dehydrogenase in 0.25 M glycine/0.5 M hydrazine/1 mM EDTA buffer at pH 9.5³³.

Luciferase assay

To analyse HIF-1 promoter activity, we performed a luciferase assay by using a plasmid vector encoding the luciferase full-length cDNA under the control of a minimal promoter containing three copies of the hypoxia response element (pRE- $\Delta\text{tk-LUC-3xHRE}$, donated by E. Berra.). Wild-type or CB_1 -KO mice astrocytes were transfected with pRE- $\Delta\text{tk-LUC-3xHRE}$ or with the empty vector at 14 DIV. After 24 h, cells were lysed and luciferase activity was determined using a Luciferase Assay System kit (Promega Biotech Iberica,) following the manufacturer's instructions. Luminescence was assessed in 96-well opaque plates (BD Falcon) using a Varioskan Flash (Thermo Fisher Scientific) spectrofluorometer. Values were normalized to those found in the cells transfected with empty vector. At least five wells were recorded per condition in each experiment ($n = 3$ experiments) and the mean values are shown.

NMR approach

Infusion. Male GFAP- CB_1 -KO mutant mice and their GFAP- CB_1 -WT littermates²¹ mice treated with vehicle or THC (10 mg/kg, i.p.) 24 h before, were used for these experiments. The mice were anesthetized with an intraperitoneal injection of a mixture containing ketamine and medetomidine (17%/83%, Virbac/Domitor, 0.2 ml/100 g body weight) before infusion of the labelled substrate in the tail vein for 1 h. The infusate solution contained [^{1-¹³C}]glucose (enriched at 99%, from Euriso-top, 750 mM). The infusate flow was monitored to obtain a time-decreasing exponential from 15 ml/h to 1.23 ml/h during the first 25 min after which the rate was kept unchanged. The blood samples were immediately mixed with 13 μl perchloric acid (11.6 M) and then centrifuged. At the end of the experiment, a sample of blood was removed; mice were rapidly euthanized by cerebral-focused microwaves (5 KW, 1 s, Sacron8000, Sairem), the only way to immediately stop all enzymatic activities and to avoid post-mortem artefacts such as anaerobic lactate production. Their brain was then rapidly removed after cutting the dome of the skull with a microcircular saw and dipped in liquid nitrogen.

Brain perchloric acid extracts. The frozen cerebral tissues were weighted and pulverized under liquid nitrogen with a mortar and pestle. A volume of 2 ml of 0.9 M perchloric acid was then added drop by drop at the nitrogen surface and the frozen droplets immediately pulverized. The mixture was transferred to a Dounce's homogenizer and homogenized at 4 °C after thawing. The suspension was then centrifuged at 4000g for 10 min. The supernatant was neutralized with KOH, centrifuged to eliminate perchlorate salts and freeze-dried. For nuclear magnetic resonance (NMR) spectroscopy, each sample was dissolved in 700 μl D₂O.

NMR spectroscopy. ¹H-NMR spectroscopy was conducted on a Bruker DPX500 wide-bore spectrometer. Spectra were acquired at 4 °C and the 90° flip angle was measured for each sample. Used parameters were: 8 s relaxation delay, 5,000 Hz sweep width and 32 K memory size, water

suppression (homonuclear presaturation). The carbon-13 specific enrichment (^{13}C -SE) of carbon position 3 for lactate (^{13}C -SE lactate C3) and that of carbon position 1 for glucose (^{13}C -SE glucose C1) were calculated based on the satellite peak areas resulting from the heteronuclear spin-coupling patterns on spectra (sera and brain samples).

Surgical procedures

Surgery for cannula implantation. Stereotaxical surgeries, performed as previously described^{45,52}, were aimed at implanting guide cannulas (Plastics One) targeting the lateral ventricles (ICV) with the following coordinates: antero-posterior (AP, -0.2), medio-lateral (ML, +/- 0.9) and dorso-ventral (DV, -2). Lactate or saline were injected using a peristaltic pump (PHD 22/2000 Syringe Pump Infusion, Harvard Apparatus, flow rate: 0.5 $\mu\text{l}/\text{min}$). The volume injected for ICV injections was 2 μl .

Surgery for viral administration. Stereotaxical surgeries, performed as previously described^{15,53}, were aimed for viral infusions in the HC and PFC. AAV vectors were injected with the help of a microsyringe attached to a pump (UMP3-1, World Precision Instruments). Mice were injected with AAV-gfa-ABC₁D-IRES-mRuby, AAV-hSyn-IRES-mRuby or AAV2/DJ-CBA-mCherry (control), AAV-gfa-ABC₁D-NDUF S4-PM-IRES-mRuby, AAV2/DJ-CBA-mCherry-miR30e-shMCT2 and AAV-hSyn-MitoCAT-IRES-mRuby viral vectors directly into the prefrontal cortex (2 injections of 1 μl per side), with the following coordinates: AP +2.9 (1st injection) and +2 (2nd injection), ML +/-1.3 (1st injection) and +/-1.5 (2nd injection), DV -2; and the hippocampus (2 injections of 1 μl per side), with the following coordinates: AP -2, ML +/-1.5, DV -2 (1st injection) and -1.5 (2nd injection), according to Paxinos and Franklin⁵⁴. Mice were used for the social interaction approach five weeks after injections for optimal expression of the viruses. mCherry or mRuby expression was checked by epifluorescence (see below) in mice used in the behavioural experiments as shown by representative images in Extended Data Figs. 4, 10c, 11. Despite the low expression of GFAP in neocortical areas⁵⁵, the use of the reduced promoter gfa-ABC₁D allowed good astroglial expression of the viruses in both HC and PFC.

Intravenous injections of AAVs. We used an adeno-associated virus (AAV) infection approach to distinguish adult astrocytes in vivo. To do this, we used the AAV-PHP.eB capsid, which efficiently transduces the central nervous system, containing GFP under the control of the short astrocyte-specific GFAP promoter (gfa-ABC₁D-GFP or gfa-ABC₁D-NDUF S4-PM) or neuron-specific synapsin promoter (hSyn-GFP). Mice were briefly anesthetized with sevoflurane (Sevorane, AbbVie) at 6% for initiation followed by around 3% for maintenance in air with supplement O₂ and NO₂ (0.4 and 0.8 l/minute, respectively) using a gas distribution column (Hersill H-3, Spain) and a vaporizer (InterMed Penlons Sigma Delta). A 50- μl aliquot of a PBS solution containing 0.1% Pluronic F-127 (Sigma-Aldrich) and AAV-PHP.eB-gfa-ABC₁D-GFP (5×10^{10} vector genomes, vg) or AAV-PHP.eB-hSyn-GFP (2×10^{10} vg) or AAV-PHP.eB-gfa-ABC₁D-NDUF S4-PM (5×10^{10} vg) was administered in the venous sinus by retro-orbital injection. The total duration of the procedure per mouse was less than 10 min, including anaesthesia and recovery. Three weeks after infection, brains were extracted and a single-cell suspension was achieved by trypsinization and smooth mechanical resuspension⁹. Despite the low expression of GFAP in neocortical areas⁵⁵, the use of the reduced gfa-ABC₁D promoter allowed good astroglial expression of the viruses in both HC and PFC. The cell suspension was incubated with different probes as described above, to assess mROS, mitochondrial membrane potential and apoptosis in GFP⁺ cells by flow cytometry.

To show representative images of this approach, three weeks following retro-orbital injection of AAVs PHP.eB-gfaABC1D-GFP or PHP.eB-hSyn-GFP, mice were euthanized by an overdose of pentobarbital and perfused transcardially with 100 ml of cold 4% paraformaldehyde (PFA) solution in phosphate buffer (PB, 0.1 M, pH 7.4). The brains were

cryoprotected in a 30% sucrose solution in PB for 24 h. Sagittal brain sections (35 μm) were cut on a freezing microtome, serially collected and stored at -20 °C until analysis. The slices were permeabilized with 0.2% Triton X-100 (Sigma-Aldrich) and blocked with 4.5% normal goat serum (Sigma-Aldrich) for 30 min and were incubated overnight at room temperature with the following primary antibodies: Phgdh (1:500, rabbit; Frontier Institute) or NeuN (1:500, mouse; Chemicon). After rinsing, the brain slices were incubated for 3 h at room temperature with fluorescent secondary 594 Alexa Fluor-conjugated antibody (Invitrogen) and mounted with FluorSave reagent (Calbiochem). Images were acquired by confocal microscopy (Leica SP8).

Immunohistochemistry and fluorescence detection

After the behavioural experiment, mice were anesthetized with chloral hydrate (400 mg/kg body weight), transcardially perfused first with phosphate-buffered solution (PB 0.1 M, pH 7.4) and then with 50 ml of 4% formaldehyde to fix tissues. After brain extraction, brain was embedded with sucrose 30% for 3 days, frozen and kept at -80 °C. Serial brain coronal cryosections were cut at 40 μm . Hippocampus and PFC sections were pre-incubated in a blocking solution of 10% donkey serum, 0.02% sodium azide and 0.3% Triton X-100 prepared in 0.1 M PB for 1 h at room temperature. All the antibodies were prepared in the blocking solution.

Staining of S100 β -mRuby. Free-floating sections were blocked with 3% H₂O₂ for 30 min and then incubated with a mix of primary antibodies: mouse monoclonal S100 β (1:1,000, Sigma-Aldrich) and rabbit polyclonal DsRed (1:1,000, Takara Bio) overnight at 4 °C. After several washes, the slices were placed for 2 h with a mix of secondary antibodies: HRP-anti mouse (1:500, Cell Signaling) and anti-rabbit Alexa Fluor 594 (1:500, Thermo Fisher Scientific). Sections were incubated with TSA FITC (1:300, 10 min, Perkin Elmer), washed, mounted, dried and coverslipped. The images were taken and analysed with an epifluorescence Leica DM6000 microscope (Leica, France).

Staining of NeuN-mRuby. Free-floating sections were incubated with a mix of primary antibodies: mouse NeuN (1:500, Sigma-Aldrich) and rabbit polyclonal DsRed (1:1,000, Takara Bio) overnight at 4 °C. After several washes, the slices were incubated for 2 h with a mix of secondary antibodies: anti-mouse Alexa Fluor 488 and anti-rabbit Alexa Fluor 594 (1:500, Thermo Fisher Scientific). Sections were washed, mounted, dried and coverslipped. The images were taken and analysed with an epifluorescence Leica DM6000 microscope (Leica, France).

Behavioural procedures

Prepulse inhibition. Prepulse inhibition (PPI) was measured in a startle chamber (SR-Lab San Diego Instruments) as described previously in the laboratory⁵². Male mice were placed in the startle chamber and a 70-dB background noise was presented during a 5-min acclimation period. The PPI session consisted of randomly presented 100 trials: a 120-dB noise trial presented alone (Startle, S), no stimulus trial, prepulse 73-dB trial, prepulse 76-dB trial, prepulse 82-dB trial, prepulse 73-dB + pulse 120-dB, prepulse 76-dB + pulse 120-dB, prepulse 82-dB + pulse 120-dB. The intervals between single trials were randomized between 10 and 30 s. The 100-ms response after the presentation of the 120-dB pulse was analysed by the PPI setting and we used the maximal response peak to calculate the PPI (% PPI = 100 \times (Startle Alone - Prepulse + Startle)/Startle Alone). THC administration (10 mg/kg, i.p.) was performed 24 h before starting the PPI experiment.

Two-chamber social interaction test. As previously described⁵², male mice were tested in an open field (35 \times 35 cm) arena with two plastic containers (plastic cylinders of 8-cm diameter with holes for odour interaction) in two opposite corners, one of them hosting a mouse (8-10-week-old adult male C57BL/6-N) and the other container

Article

remaining empty. In each corner we defined the 'social' and 'non-social' zones as an 8-cm area surrounding the containers. For each experimental group, mice were put in the middle of the open field for 5 min and the position of the container with the mouse was counterbalanced. A ceiling-mounted camera recorded mouse movements. Male mice were used and THC (10 mg/kg, i.p.) or its vehicle were administered 24 h before the task. A social interaction index was calculated as time spent in the social zone divided by the total time spent in both zones⁵².

Direct social interaction test. Cannulated adult male mice were tested in 35.5 × 23.5 × 19 cm cages at 20 ± 2 lux with fresh bedding and video recorded using a Blackfly S digital camera. Each subject mouse was matched with a stimulus mouse in age and weight, which was habituated to the testing cage for 10 min the day prior. Subject mice were injected intraventricularly with 2 µl of saline or lactate (100 mM) solutions in an adjacent room just before the test. The test (adapted from a previous study⁵⁶) consists of 3 trials preceded by a 5-min habituation to the testing cage, during which subject mice were allowed to explore the empty testing cage freely. Immediately afterwards, a stimulus male mouse was introduced in the cage for 1-min direct interaction. After each trial, the stimulus mouse was moved back to its home cage during the 2-min intertrial time. We repeated this for 3 trials with an intertrial time of 2 min. Social behaviours were manually scored offline by a blinded experimenter. Mice that fought in more than one trial were excluded from the analysis. THC (10 mg/kg, i.p.) or its corresponding vehicle were administered 24 h before the task.

Open-field test. Mice were placed in an open field (width, 60 cm; length, 60 cm) the bottom of which was divided into squares. A ceiling-mounted camera recorded mouse movements. Total number of crossed squares and the time spent in the centre of the open field were measured manually during 5 min by the researcher in a different room. Mice were treated with THC (10 mg/kg) or vehicle 24 h before the experiment.

Elevated plus maze. The elevated plus maze consisted of four elevated arms (height, 66 cm; length, 45 cm; width, 10 cm). The arms were arranged in a cross-like configuration, with two opposite arms being enclosed by 50-cm high walls and the two other arms being open. The four arms were connected by a squared central platform (10 cm × 10 cm). Both the central platform and the open arms were under bright illumination (100–120 lux), whereas the closed arms were under weak illumination (30 lux). Each mouse was placed on the central platform, facing an open arm. The time spent on the open arms were recorded for 5 min in mice receiving vehicle or THC (10 mg/kg, i.p.) 24 h before the experiment.

Spontaneous alternation. Spontaneous alternation was assessed in a Y-maze (42 cm long, 8 cm wide, 120° between arms) in a room with 50 lux of light containing a ceiling-mounted camera. Mice were placed in one of the arms for 8 min and scored for each entry when all four paws were placed in one of the arms. GFAP-*CB₁*-WT and GFAP-*CB₁*-KO mice were treated with an injection of THC (10 mg/kg) or vehicle 24 h before entering the Y-maze. The percentage of alternation was calculated as: [number of correct triplets/(total number of arm entries – 2)] × 100.

Statistical analysis

No statistical methods were used to predetermine sample size. All results are expressed as the mean values ± s.e.m. For the electron microscopy experiments, we used ANOVA analysis to compare all experimental groups for each brain region followed by Bonferroni test. For the in vitro experiments, to compare the values between genotypes we used a Student's *t*-test. For the multiple values comparisons, we used a one-way or two-way ANOVA followed by Bonferroni test. For the NMR experiments we used a non-paired *t*-test between the two experimental groups. For the behavioural experiments, we used a

two-way ANOVA followed by Bonferroni test (for example, social index) or paired *t*-test (for example, exploration time) when an interaction was found. A one-way ANOVA was also used to analyse possible differences between control groups. All the statistical analysis was performed using SPSS v.16.0 or GraphPad Prism software for Macintosh. In all cases, *P* < 0.05 was considered significant and the exact *P* value is shown except when the statistical software is just providing a range. When normalization was required in some in vitro measurements, the statistics were performed on the raw data presented in the source data files. Representative immunoblot or immunochemistry images represent experiments repeated at least three times with similar results. All molecular experiments were repeated three to five times and behavioural experiments were also repeated two or three times in independent groups of mice with similar results. Additional statistical details and original gels can be found in the Supplementary Information.

Reporting summary

Further information on research design is available in the Nature Research Reporting Summary linked to this paper.

Data availability

All data generated in this manuscript are included within the paper (and its Supplementary Information files). For any further inquiries about our work please contact the corresponding authors. Source data are provided with this paper.

1. Melsner, S. et al. Functional analysis of mitochondrial CB1 cannabinoid receptors (mtCB1) in the brain. *Methods Enzymol.* **593**, 143–174 (2017).
2. Jollé, C., Déglon, N., Pythoud, C., Bouzier-Sore, A. K. & Pellerin, L. Development of AAV2/DJ-based viral vectors to selectively downregulate the expression of neuronal or astrocytic target proteins in the rat central nervous system. *Front Mol. Neurosci.* **12**, 201 (2019).
3. Marsicano, G. et al. The endogenous cannabinoid system controls extinction of aversive memories. *Nature* **418**, 530–534 (2002).
4. Puente, N., Bonilla-Del Río, I., Achicallende, S., Nahirney, P. C. & Grandes, P. High-resolution immunoelectron microscopy techniques for revealing distinct subcellular type 1 cannabinoid receptor domains in brain. *Bio-protocols* **9**, e3145 (2019).
5. De Rasmio, D. et al. Activation of the cAMP cascade in human fibroblast cultures rescues the activity of oxidatively damaged complex I. *Free Radic. Biol. Med.* **52**, 757–764 (2012).
6. Acín-Pérez, R., Fernández-Silva, P., Peleato, M. L., Pérez-Martos, A. & Enriquez, J. A. Respiratory active mitochondrial supercomplexes. *Mol. Cell* **32**, 529–539 (2008).
7. Belousov, V. V. et al. Genetically encoded fluorescent indicator for intracellular hydrogen peroxide. *Nat. Methods* **3**, 281–286 (2006).
8. Darley-Usmar, V. M., Rickwood, D. & Wilson, M. T. (eds) *Mitochondria: A Practical Approach* (IRL, 1987).
9. King, T. E. in *Methods in Enzymology* Vol. 10 (eds Estabrook, R. W. & Pullman, M. E.) 216–225 (Academic, 1967).
10. Wharton, D. C. & Tzagoloff, A. in *Methods in Enzymology* Vol. 10 (eds Estabrook, R. W. & Pullman, M. E.) 245–250 (Academic, 1967).
11. Shepherd, D. & Garland, P. B. The kinetic properties of citrate synthase from rat liver mitochondria. *Biochem. J.* **114**, 597–610 (1969).
12. Busquets-García, A. et al. Pregnenolone blocks cannabinoid-induced acute psychotic-like states in mice. *Mol. Psychiatry* **22**, 1594–1603 (2017).
13. Soria-Gómez, E. et al. Habenular CB₁ receptors control the expression of aversive memories. *Neuron* **88**, 306–313 (2015).
14. Paxinos, G. & Franklin, K. B. J. *The Mouse Brain in Stereotaxic Coordinates* (Academic, 2001).
15. Martin, P. M. & O'Callaghan, J. P. A direct comparison of GFAP immunocytochemistry and GFAP concentration in various regions of ethanol-fixed rat and mouse brain. *J. Neurosci. Methods* **58**, 181–192 (1995).
16. Huang, H. et al. Chronic and acute intranasal oxytocin produce divergent social effects in mice. *Neuropsychopharmacol.* **39**, 1102–1114 (2014).

Acknowledgements We thank D. Gonzales, N. Aubailly, M. Carabias-Carrasco, L. Martin, E. Prieto-García and all the personnel of the Animal Facilities of the NeuroCentre Magendie and University of Salamanca for mouse care; the Biochemistry Platform of Bordeaux NeuroCampus for help; S. Papa and D. De Rasmio for providing the NDUFS4 cDNA and anti-phospho-Ser173 NDUFS4 antibody, respectively; the viral vector facility headed by A. Bemelmans for producing AAVs at MIRGen; M.-C. Gaillard for help in the design and production of the gfaABC1D-NDUFS4-PM plasmid; P.-A. Vigneron for the acquisition of confocal images depicting cellular tropism of AAV PHP.eB; all the members of the Marsicano laboratory for useful discussions; V. Morales for invaluable assistance; and S. Pouvreau, G. Benard, D. Cota and G. Ferreira for critical reading of the manuscript and suggestions. This work was funded by: INSERM, the European Research Council (Endofood, ERC-2010-StG-260515 and CannaPreg, ERC-2014-PoC-640923, MiCaBra, ERC-2017-AdG-786467), Fondation pour la Recherche Médicale (FRM, DRM20101220445), the Human Frontiers Science Program,

Region Nouvelle Aquitaine and Agence Nationale de la Recherche (ANR; NeuroNutriSens ANR-13-BSV4-0006, CaCoV1 ANR 18-CE16-0001-02, MitObesity ANR 18-CE14-0029-01, ORUPS ANR-16-CE37-0010-01 and BRAIN ANR-10-LABX-0043) (to G.M.); NIH/NIDA (1R21DA037678-01), Spanish Ministry of Science, Innovation and Universities (MCINU/FEDER; grants SAF2016-78114-R and RED2018-102576-T), Instituto de Salud Carlos III (CB16/10/00282), an EU BATCure grant (666918), Junta de Castilla y León (Escalera de Excelencia CLU-2017-03), Ayudas Equipos Investigación Biomedicina 2017 Fundación BBVA and Fundación Ramón Areces (to J.P.B.); Instituto de Salud Carlos III (PI18/00285; RD16/0019/0018), the European Regional Development Fund, the European Union's Horizon 2020 Research and Innovation Programme (grant agreement 686009), Junta de Castilla y León (IES007P17) and Fundación Ramón Areces to (A.A.); French State/ANR/IdEx (ANR-10-IDEX-03-02), Eu-Fp7 (FP7-PEOPLE-2013-IEF-623638) and Ramon y Cajal Investigator Program (RYC-2017-21776) (to A.B.-G.); FRM (SPF20121226369) (to R.S.); FRM (ARF20140129235) (to L.B.); Spanish Ministry of Science, Innovation and Universities (MCINU/FEDER; grants SAF2015-64945-R and RTI2018-095311-B-I00) (to M.G.); Canada Research Chair, Alzheimer Society of Canada—Brain Canada (17-09), Natural Sciences and Engineering Research Council (RGPIN-2015-05880), Canadian Breast Cancer Foundation (2015-317342), Canadian Health Research Institute (CIHR, 388808), New Brunswick Innovation Foundation, New Brunswick Health Research Foundation and Université de Moncton (to E.H.-C.); Basque Government (IT1230-19), Red de Trastornos Adictivos, Instituto de Salud Carlos III (ISC-III), European Regional Development Funds-European Union (ERDF-EU; RD16/0017/0012) and MINECO/FEDER, UE (SAF2015-65034-R) (to P.G.); University of the Basque Country PhD contract (PIF 16/251) (to S.A.); POP contract (BES-2016-076766, BES-C-2016-0051) (to I.B.-D.R.); French State/ANR (ANR-10-IDEX and TRAIL ANR-10-LABX-57); French-Swiss ANR-FNS (ANR-15-CE37-0012)

(to A.-K.B.-S.); SFB/TRR 58 'Fear, anxiety, anxiety disorders' (subproject A04); and CRC 1193 'Neurobiology of resilience' (subproject B04) (to B.L.).

Author contributions J.P.B. and G.M. conceptualized and supervised the study. D.J.-B., E.H.-C., C.V.-G., R.S., I.L.-F., M.R.-B., D.S. and A.A. performed and supervised in vitro experiments in cell and astrocyte cultures and ex vivo analysis of brain tissue; A.B.-G., C.I. and P.G.-S. performed behavioural experiments and surgical procedures in mice; E.R. and M.G. provided some CB₁-KO mice to the group of J.P.B.; D.A. and A.P. performed electrophysiological experiments not shown in the manuscript; M.V. and F.J.-K. performed mouse perfusion and immunohistochemistry experiments; A.C. and L.B. produced some of the viral constructs used (for example, Syn-MitoCAT); I.B.-D.R., N.P., S.A. and P.G. performed and supervised electron microscopy experiments; M.-L.L.-R. provided pharmacological tools (HU210-Biotin); C. Jollé, N.D. and L.P. provided specific viral constructs to modulate the MCT2 transporter; C. Josephine and G.B. provided data and viral vectors for mouse retro-orbital injections; B.L. and P.-V.P. provided conceptual ideas; and A.-K.B.-S. performed in vivo NMR experiments. D.J.-B., A.B.-G., E.H.-C., M.G., J.P.B. and G.M. wrote the paper with input from all authors.

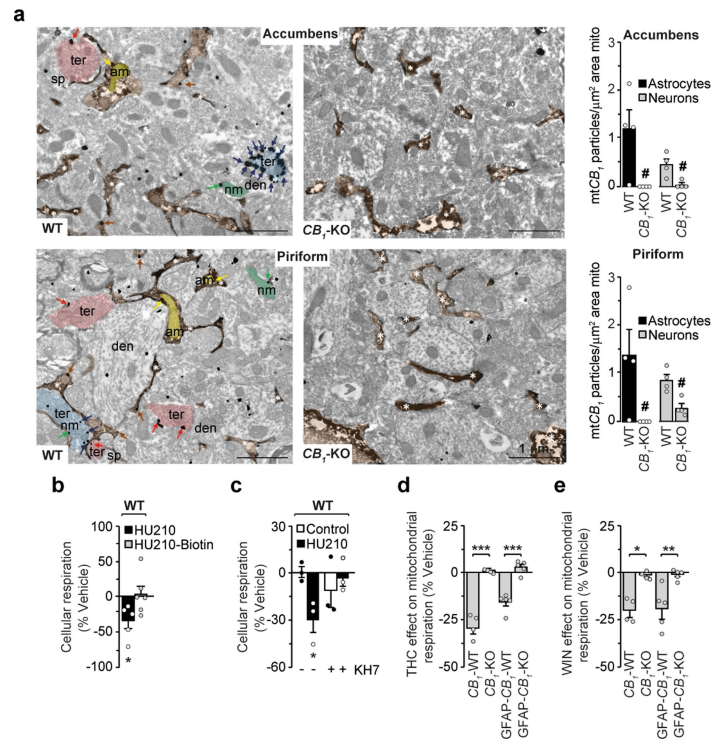
Competing interests The authors declare no competing interests.

Additional information

Supplementary information is available for this paper at <https://doi.org/10.1038/s41586-020-2470-y>.

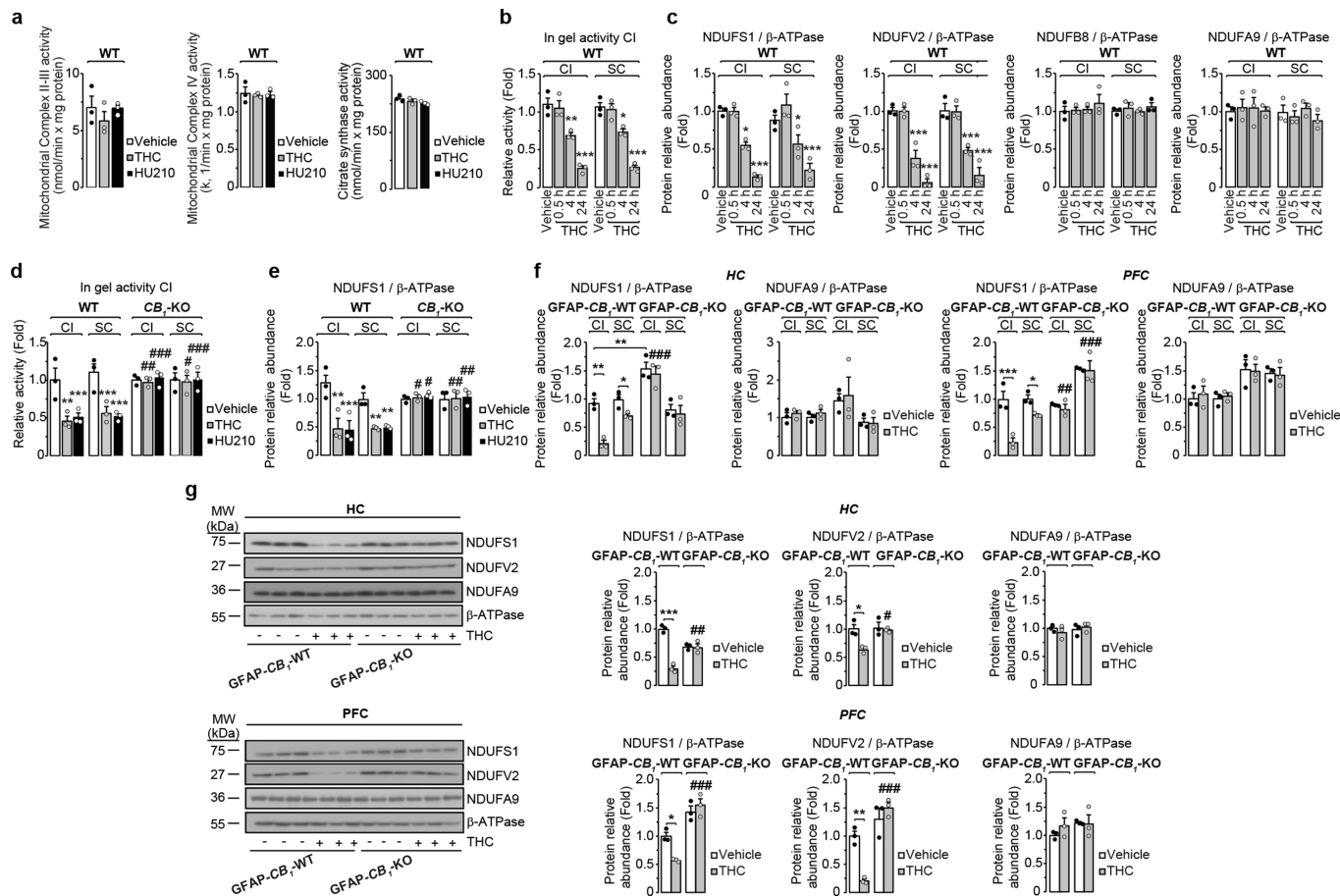
Correspondence and requests for materials should be addressed to J.P.B. or G.M.

Reprints and permissions information is available at <http://www.nature.com/reprints>.



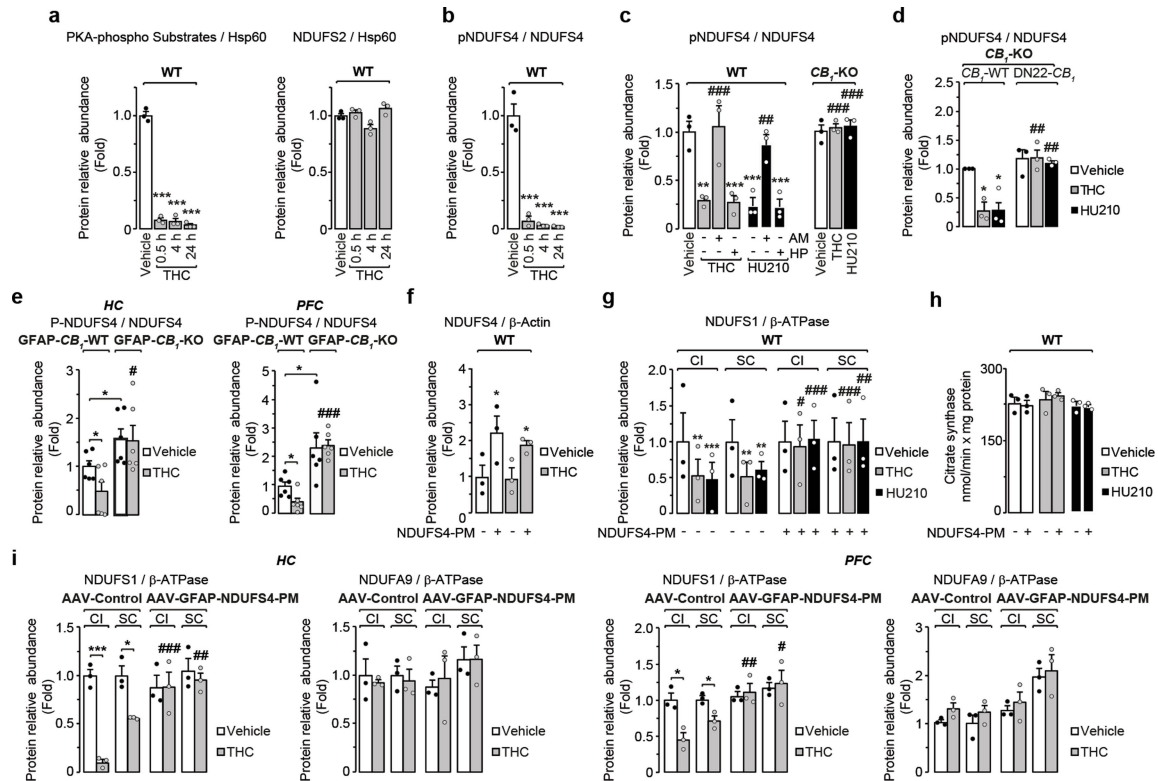
Extended Data Fig. 1 | Role of astroglial mtCB₁ in the cannabinoid-induced decrease of respiration in forebrain mitochondria. **a**, Detection of CB₁ receptors on astroglial and neuronal mitochondrial membranes in the nucleus accumbens and piriform cortex of wild-type and CB₁-KO mice ($n = 4$). am, astrocytic mitochondria; nm, neuronal mitochondria; sp, spine; ter, terminal. CB₁-positive inhibitory terminals are marked in blue, astrocytes in brown, excitatory terminals in red, astrocytic mitochondria in yellow and neuronal mitochondria in green. Asterisks indicate astrocytic processes; coloured arrows point to CB₁ particles at colour-matching subcellular compartments and mitochondria. Scale bars, 1 μm. #, $P < 0.05$ (vs WT). **b**, Effects of the CB₁ receptor cell permeant and impermeant agonists HU210 (1 μM, $n = 5$) and

HU210-Biotin (1 μM, $n = 6$), respectively, on cellular respiration of primary mouse cortical astrocyte cultures. *, $P < 0.05$ (versus HU210-Biotin). **c**, sAC inhibitor KH7 (5 μM, $n = 3$) effects on the HU210-induced reduction of cellular respiration in astrocyte cultures. *, $P < 0.05$ (versus control). **d**, **e**, THC (800 nM) (**d**) and WIN (100 nM) (**e**) effects on respiration of purified brain mitochondria from CB₁-KO ($n = 4$) and GFAP-CB₁-KO ($n = 5$) mice and their respective WT littermates (CB₁-WT and GFAP-CB₁-WT). *, $P < 0.05$; **, $P < 0.01$; ***, $P < 0.001$ (versus WT conditions). Data are expressed as mean ± s.e.m. and are analysed by one-way ANOVA in **a**, **d** and **e**; two-way ANOVA in **c** and unpaired two-sided Student's *t*-test in **b** and **c**. *n* represents number of mice in **a**, **d** and **e** and independent experiments in **b** and **c**. Statistical details, Supplementary Table 2.



Extended Data Fig. 2 | Activation of mtCB₁ receptors inhibits complex I activity by destabilizing the N-module of complex I. **a**, THC (1 μ M) or HU210 (50 nM) effects on complex II–III (CII–III; left), complex IV (CIV; centre) and citrate synthase (right) activities in WT astrocyte cultures ($n = 3$). **b**, **c**, Quantification ($n = 3$) of gels represented in Fig. 1c, reporting the effects of THC on **(b)** mitochondrial complex I (CI) activity and **(c)** expression (normalized to β -ATPase) of the complex I subunits NDUFS1, NDUFV2, NDUFB8 and NDUFA9 in complex I and super-complexes (SC) of cultured astrocytes from WT mice. *, $P < 0.05$; **, $P < 0.01$; ***, $P < 0.001$ (versus Vehicle). **d**, **e**, Quantification ($n = 3$) of gels represented in Fig. 1d, reporting THC or HU210 effects on **(d)** complex I activity and **(e)** expression (normalized to β -ATPase) of the complex I subunit NDUFS1 in complex I and SC of WT and CB₁-KO mice. **, $P < 0.01$; ***, $P < 0.001$ (versus Vehicle); #, $P < 0.05$; ##, $P < 0.01$; ###, $P < 0.001$ (versus WT). **f**, Relative quantification ($n = 3$) of BNGE represented in Fig. 1e, reporting the

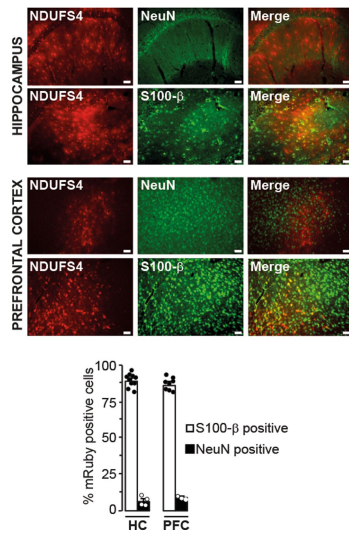
in vivo THC effects (10 mg/Kg, 24h before) on complex I activity and expression (normalized to β -ATPase) of the complex I subunit NDUFS1 and NDUFA9 in complex I and SC of HC (left panels) or PFC (right panels) from GFAP-CB₁-WT and GFAP-CB₁-KO mice. *, $P < 0.05$; **, $P < 0.01$; ***, $P < 0.001$; ##, $P < 0.01$; ###, $P < 0.001$ (versus WT). **g**, Representative Western Immunoblottings (left) and relative quantification of these gels ($n = 3$) (right) showing the effects of in vivo THC treatment (10 mg/Kg, 24h before) on expression of the complex I subunits NDUFS1, NDUFV2 and NDUFA9 of HC or PFC from GFAP-CB₁-WT and GFAP-CB₁-KO mice. *, $P < 0.05$; **, $P < 0.01$; ***, $P < 0.001$; #, $P < 0.05$; ##, $P < 0.01$; ###, $P < 0.001$ (versus WT). Data are expressed as mean \pm s.e.m. and are analysed by one-way ANOVA in **a–c** and two-way ANOVA in **d–g**. n represents number of independent experiments. Original gels, Supplementary Fig. 1; Statistical details, Supplementary Table 2.



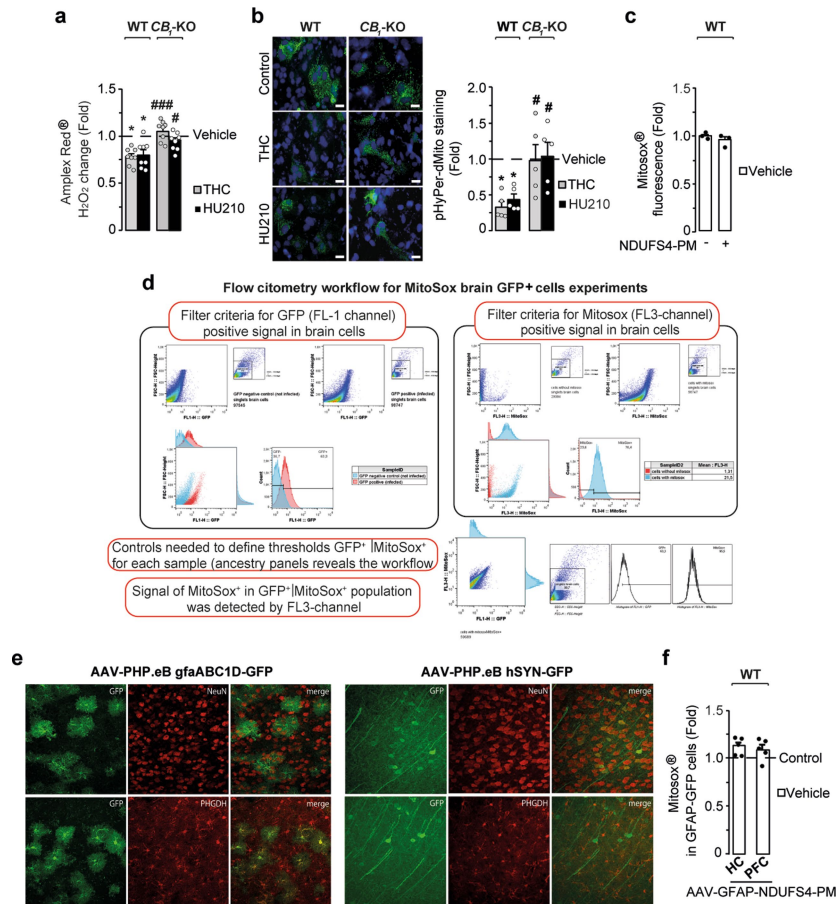
Extended Data Fig. 3 | Activation of astroglial mtCB₁ receptors decreases NDUFS4-Ser173 phosphorylation to inhibit complex I activity.

a, Quantification ($n = 3$) of Fig. 2a, reporting the THC (1 μ M) effects on PKA-dependent phosphorylation of complex I proteins (left) and on NDUFS2 levels in WT astrocytes (right). ***, $P < 0.001$ (versus Vehicle). **b**, Quantification ($n = 3$) of Fig. 2b, reporting the THC effects on pNDUFS4 in WT astrocytes. ***, $P < 0.001$ (versus Vehicle). **c**, Quantification ($n = 3$) of Fig. 2c, reporting THC or HU210 effects on pNDUFS4 levels in WT and *CB₁-KO* astrocytes. **, $P < 0.01$; ***, $P < 0.001$ (versus Vehicle). ###, $P < 0.001$ (versus WT-THC). **d**, Quantification ($n = 3$) of Fig. 2d, reporting THC or HU210 effects on pNDUFS4 levels in *CB₁-KO* astrocytes (empty, *CB₁-WT*, DN22-*CB₁*). *, $P < 0.05$ (versus Vehicle). ##, $P < 0.01$ (versus WT). ###, $P < 0.001$ (versus WT-THC). **e**, Quantification ($n = 3$) of Fig. 2e, reporting THC (10 mg/Kg, 24h before) effects on pNDUFS4 of HC (left) or PFC (right) from GFAP-*CB₁*-WT and GFAP-*CB₁*-KO mice. *, $P < 0.05$ (versus Vehicle). #, $P < 0.05$; ###, $P < 0.001$ (versus WT). **f**, Quantification ($n = 3$) of Fig. 2f, reporting the

expression of NDUFS4-PM in WT astrocytes with or without THC treatment. *, $P < 0.05$ (versus Vehicle). **g**, Quantification ($n = 3$) of Fig. 2g, reporting NDUFS4-PM expression in WT astrocytes effects on complex I activity, NDUFS1 levels and β -ATPase expression after 24h incubation with vehicle, THC or HU210. **, $P < 0.01$; ***, $P < 0.001$ (versus Vehicle). #, $P < 0.05$; ##, $P < 0.01$; ###, $P < 0.001$ (versus empty). **h**, THC or HU210 effects on citrate synthase activity of WT astrocytes in the presence or absence of NDUFS4-PM ($n = 3$). **i**, Quantification of Fig. 2i, reporting AAV-GFAP-NDUFS4-PM effects on complex I activity, NDUFS1 and NDUFA9 levels and -ATPase expression in HC (left) and PFC (right) 24h after THC treatment (10 mg/Kg). *, $P < 0.05$; ***, $P < 0.001$ (versus Vehicle). #, $P < 0.05$; ##, $P < 0.01$; ###, $P < 0.001$ (vs AAV-Control). Data are expressed as mean \pm s.e.m. and are analysed by one-way ANOVA in **a**, **b** and two-way ANOVA in **c**-**i**. n represents number of independent experiments. Statistical details, Supplementary Table 2.

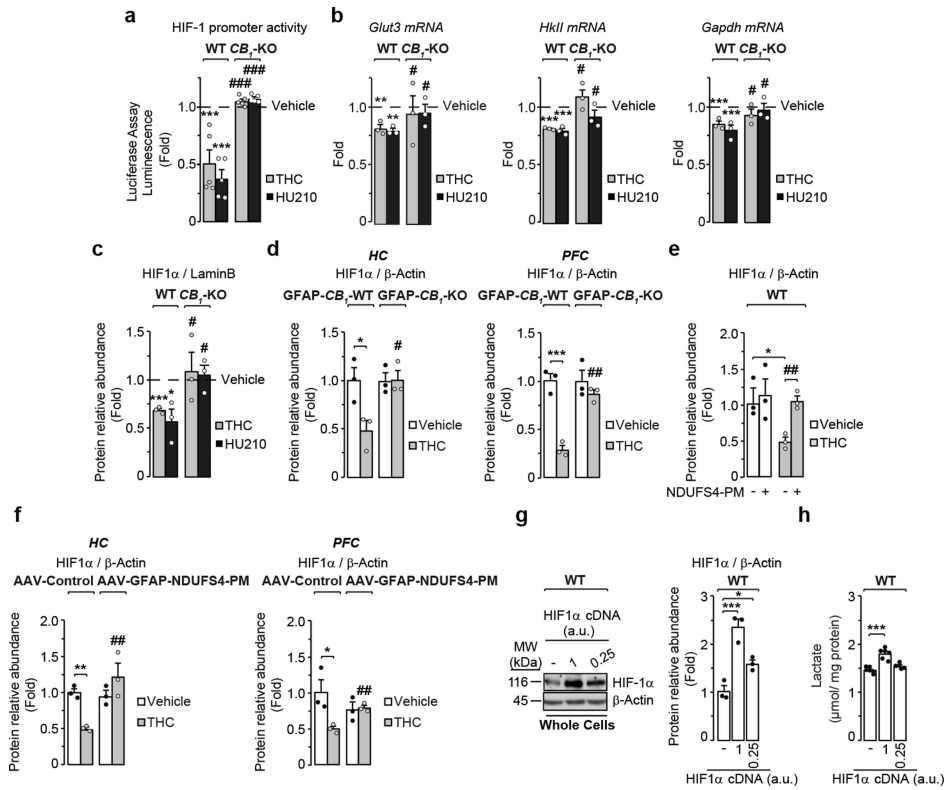


Extended Data Fig. 4 | Astroglial expression of NDUFS4-PM in the hippocampus and PFC. Top, immunofluorescence micrographs showing the expression of AAV-gfa-ABC₁D-NDUFS4-PM (fused to mRuby, red) in neurons (staining with NeuN marker, green) or astrocytes (staining with an anti-S-100β antibody, green) of the HC and the PFC. Note the large overlapping in the merged images when using the S-100-β antibody (HC, *n* = 10 mice; PFC, *n* = 8) but not the neuronal NeuN marker (*n* = 5 mice; PFC, *n* = 3). Bottom, graph quantification showing the percentage of mRuby positive cells (NDUFS4-PM positive) that colocalize with the astroglial marker S-100-β or the neuronal one NeuN. Data are expressed as mean ± s.e.m. Scale bars, 40 μm.



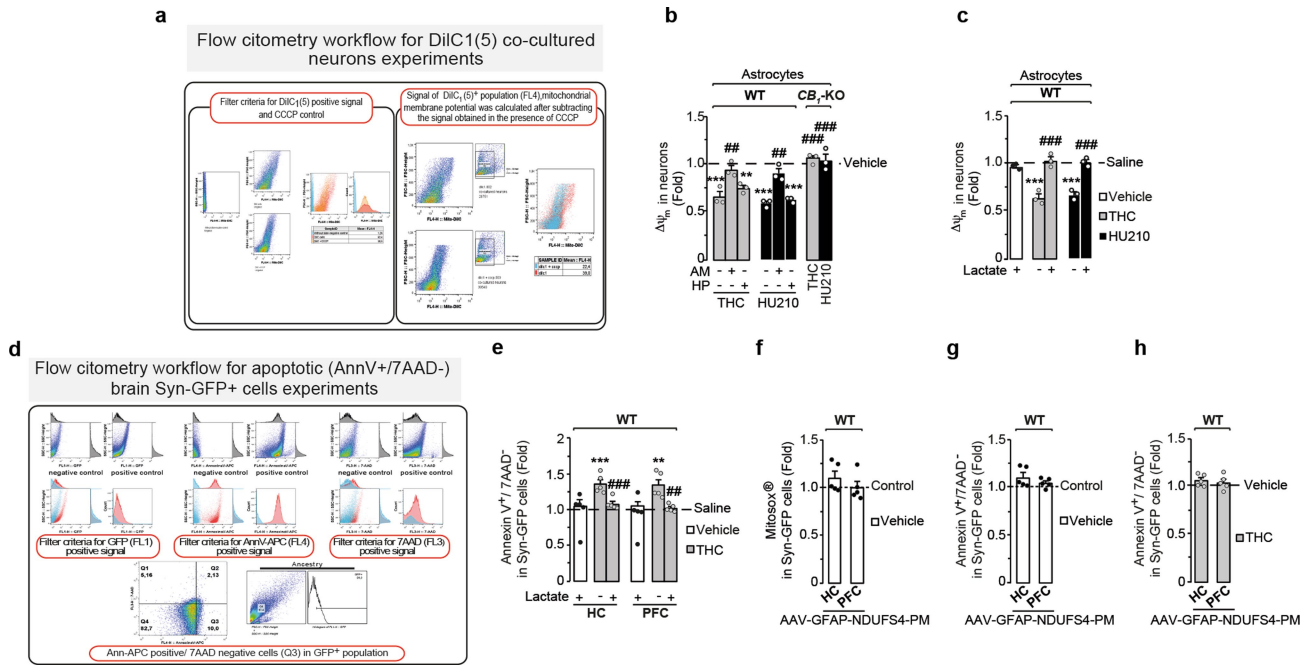
Extended Data Fig. 5 | MtCB₁-dependent effects on mROS and mitochondrial membrane potential in astrocytes. **a**, THC (1 μM) or HU210 (50 nM) effects on mROS in *CB₁*-WT and *CB₁*-KO astrocytes (*n* = 8) as revealed by Amplex Red fluorescence. *, *P* < 0.05 (versus Vehicle); #, *P* < 0.05; ###, *P* < 0.001 (versus WT). **b**, pHyPer-dMito micrographs (left) and quantification (right) 24h after THC (1 μM) or HU210 (50 nM) treatments in *CB₁*-WT and *CB₁*-KO astrocytes (*n* = 5). Scale bar: 40 μM. *, *P* < 0.05 (versus Vehicle); #, *P* < 0.05 (versus WT). **c**, Effects on mROS of NDUFS4-PM transfection per se in astrocytes from *CB₁*-WT (*n* = 3). **d**, MitoSOX schematic example of the gating strategy and workflow for the determination of mROS in GFP+ cells by flow cytometry. **e**, Left,

immunofluorescence micrographs showing expression of GFP three weeks after retro-orbital injection of the AAV-PHP.eB gfaABC1D-GFP. GFP is expressed in PHGDH-positive astrocytes but not in NeuN-positive neurons (*n* = 3). Right, immunofluorescence micrographs showing expression of GFP three weeks after retro-orbital injection of the AAV-PHP.eB hSYN-GFP. GFP is expressed in NeuN-positive neurons and not in PHGDH-positive astrocytes (*n* = 3). **f**, AAV-gfa-ABC1D-NDUFS4-PM infusion effects on the levels of mROS in HC and PFC (*n* = 5). Data are expressed as mean ± s.e.m. and are analysed by two-way ANOVA. *n* represents number of independent experiments. Statistical details are in Supplementary Table 2.



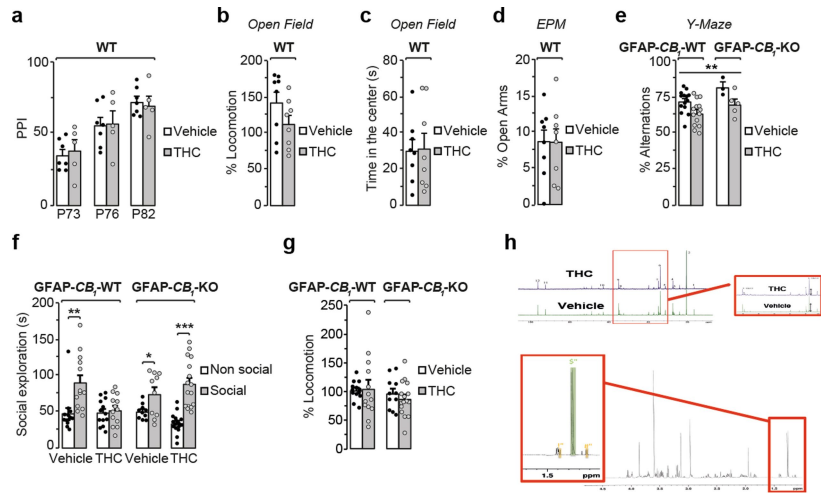
Extended Data Fig. 6 | Activation of astroglial mtCB₁ receptors decreases glycolysis and lactate release by attenuating the HIF-1 pathway. **a**, THC (1 μ M) or HU210 (50 nM) effects on HIF-1 promoter activity in WT and *CB₁*-KO astrocytes ($n=5$). ***, $P < 0.001$ (versus Vehicle); ###, $P < 0.001$ (versus WT). **b**, THC or HU210 effects ($n=3$) on mRNA levels of different HIF-1 targets (*Glut3*, *HkII* and *Gapdh*) in WT and *CB₁*-KO astrocytes. **, $P < 0.01$; ***, $P < 0.001$ (versus Vehicle); #, $P < 0.05$ (versus WT). **c**, Quantification ($n=3$) of Fig. 3g, reporting THC and HU210 effects on HIF-1 α nuclear expression in WT and *CB₁*-KO astrocytes. *, $P < 0.05$; ***, $P < 0.001$ (versus Vehicle); #, $P < 0.05$; (versus WT). **d**, Quantification ($n=3$) of Fig. 3h, reporting THC effects (10 mg/Kg, 24h before) on HIF-1 α protein levels in HC (left) or PFC (right) from GFAP-*CB₁*-WT and GFAP-*CB₁*-KO mice. *, $P < 0.05$; ***, $P < 0.001$ (versus Vehicle); #, $P < 0.05$; ##, $P < 0.01$ (versus WT). **e**, Quantification ($n=3$) of Fig. 3i, reporting NDUFS4-PM

expression effects on the THC-induced HIF-1 α expression decrease in WT astrocytes. *, $P < 0.05$ (versus Vehicle); ##, $P < 0.01$ (versus empty). **f**, Quantification ($n=3$) of Fig. 3j, reporting the effect of local infusion of AAV-GFAP-NDUFS4-PM on the THC-mediated decrease of HIF-1 α in HC (left) and PFC (right) from WT mice. *, $P < 0.05$; **, $P < 0.01$ (versus Vehicle); ##, $P < 0.01$ (versus AAV-Control). **g**, Western immunoblotting (left) and quantification ($n=3$, right) showing the HIF-1 α overexpression obtained by transfecting astrocytes with 1 or 0.25 μ g plasmid DNA, respectively. *, $P < 0.05$; ***, $P < 0.001$ (versus empty). **h**, Effect of HIF-1 α overexpression ($n=6$) on lactate release from WT astrocytes. ***, $P < 0.001$ (versus empty). Data are expressed as mean \pm s.e.m. and are analysed by one-way ANOVA in **g-h** and two-way ANOVA in **a-f**. n represents number of independent experiments. Statistical details, Supplementary Table 2.



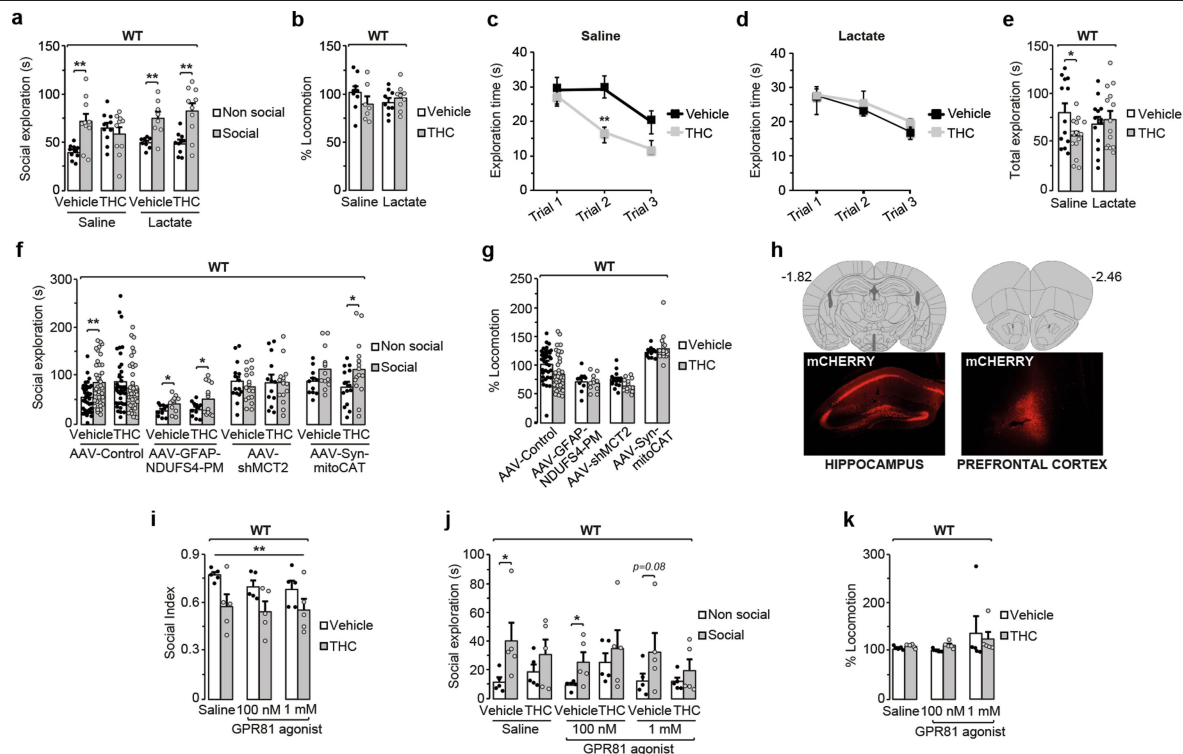
Extended Data Fig. 7 | Determination of mitochondrial membrane potential and apoptosis in neurons. **a**, Schematic and representative example of the gating strategy and workflow for the determination of mitochondrial membrane potential (DiIC1(5)) in neurons co-cultured with astrocytes by flow cytometry. **b**, Effects on cultured neurons co-cultured with astrocytes from *CB1*-WT or *CB1*-KO mice previously treated with THC (1 μ M) or HU210 (50 nM) on mitochondrial membrane potential ($\Delta\Psi_m$). **, $P < 0.01$; ***, $P < 0.001$ (versus Vehicle); ##, $P < 0.01$; ###, $P < 0.001$ (versus WT-cannabinoids). **c**, Effects of lactate supplementation (2 mM) on the decreased mitochondrial membrane potential ($\Delta\Psi_m$). ***, $P < 0.001$ (versus Saline); ###, $P < 0.001$; (versus cannabinoids). **d**, Schematic and representative example of the gating strategy and workflow for the determination of apoptosis (AnnV+/7AAD) in brain GFP+ cells by flow cytometry. **e**, Effects of ICV

lactate supplementation (100 mM) on the THC-induced increase of apoptotic cell death, in Syn-positive cells (neurons) from PFC or HC ($n = 5$). **, $P < 0.01$; ***, $P < 0.001$ (versus Saline); ##, $P < 0.01$; ###, $P < 0.001$ (versus THC). **f**, Effect of the intravenous administration of AAV-gfa-ABC₁D-NDUFS4-PM on the neuronal levels of mROS as revealed by MitoSOX analysis by fluorescence-activated cell sorting ($n = 5$) (f) and the apoptotic cell death in neurons as revealed by cell sorting flow cytometry ($n = 5$) (g). **h**, Effects of retro-orbital injection of AAV-PHP.eB-gfa-ABC₁D-NDUFS4-PM on the THC-induced increase of apoptotic cell death, in Syn-positive cells (neurons) from PFC or HC ($n = 5$). Data are expressed as mean \pm s.e.m. and are analysed by one-way ANOVA in **b** and two-way ANOVA in **c** and **e**. n represents number of independent experiments. Statistical details, Supplementary Table 2.



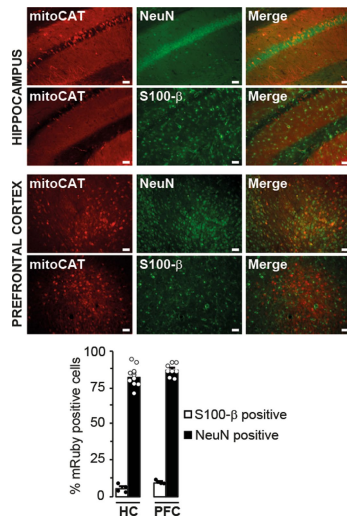
Extended Data Fig. 8 | Behavioural and metabolic effects of THC administration in GFAP-CB₁-KO mice. **a-d**, The administration of THC (10 mg per kg, i.p.) did not affect the prepulse inhibition (PPI) of the startle response (**a**, Veh, $n = 7$; THC, $n = 5$), the locomotion assessed in the Open Field (**b**, $n = 8$), the anxiety-like responses assessed in the Open Field (**c**, $n = 8$) or in the elevated plus maze (**d**, $n = 8$). **e**, THC induced spontaneous alternation impairment in both in GFAP-CB₁-WT ($n = 15$) and GFAP-CB₁-KO mice ($n = \text{Veh}, n = 3$; THC, $n = 5$). $**P < 0.01$ (versus Vehicle). **f**, THC effects (Fig. 4k) on the exploration times of social and non-social compartments in GFAP-CB₁-KO mice (Veh, $n = 11$; THC, $n = 16$) and GFAP-CB₁-WT ($n = 13$) littermates. $*$, $P < 0.05$; $**$, $P < 0.01$; $***$, $P < 0.001$ (versus non-social). **g**, Locomotor effects of THC in the sociability test in GFAP-CB₁-KO mice (Veh, $n = 11$; THC, $n = 16$) and GFAP-CB₁-WT littermates

($n = 13$). **h**, Top, typical ¹³C-NMR spectra of brain perchloric acid extracts of a control mouse treated with Vehicle (green) or THC (blue). 1: Alanine C3; 2: Lactate C3; 3: Glutamine C3; 4: Glutamate C3; 5: Glutamine C4; 6: Glutamate C4; 7: GABA C2; 8: Glutamine C2; 9: Glutamate C2; 10: Ethylene glycol (external standard); 11: α Glucose C1; 12: β Glucose C1. Right, zoom showing the difference in the incorporation of carbone-13 into carbone 2 compared to carbone 4 between vehicle- and THC-treated. Black arrow represents the height of carbone-2 peak. Bottom, typical raw ¹H-NMR spectra of brain perchloric acid extracts of vehicle treated mouse. Data are expressed as mean \pm s.e.m. and are analysed by two-way ANOVA in **e**, **f**. n represents number of mice. Experiments shown in **h**, **i** were repeated in four independent experiments. Statistical details, Supplementary Table 2.

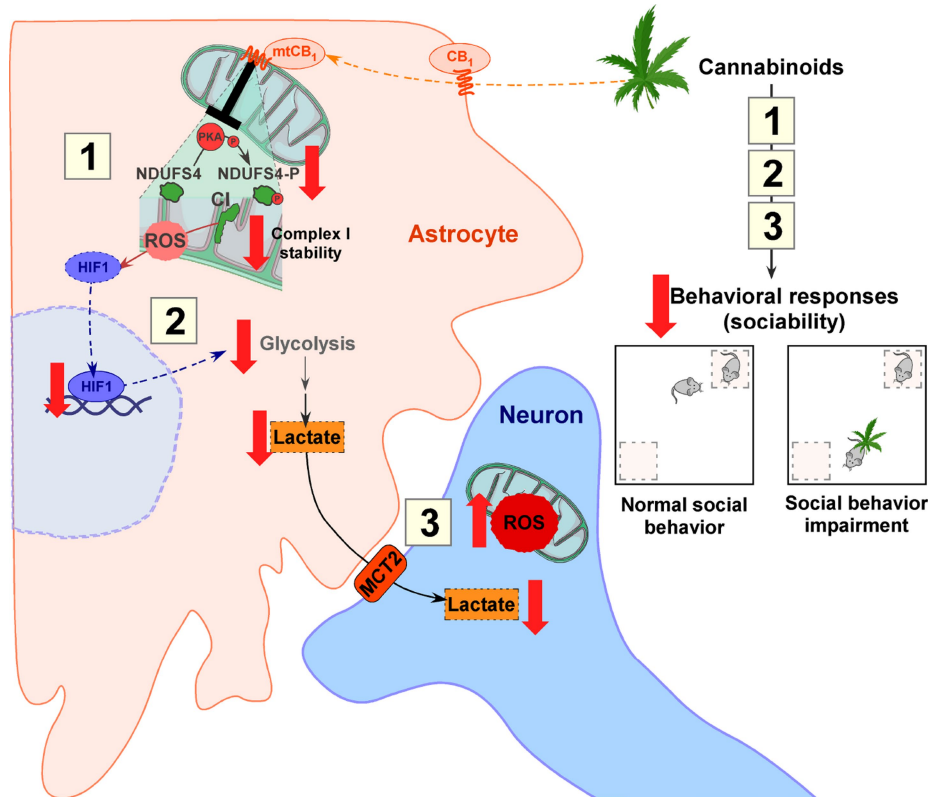


Extended Data Fig. 9 | Mechanisms that underlie the THC-induced impairment of social interaction. **a**, THC effects (Fig. 4m) on exploration times of social and non-social compartments (Sal-Veh, $n = 10$; Sal-THC, $n = 8$; Lac-Veh, $n = 10$; Lac-THC, $n = 10$). **, $P < 0.01$ (versus non-social). **b**, Locomotor effects of THC in the sociability test in mice receiving saline or lactate (Sal-Veh, $n = 9$; Sal-THC, $n = 7$; Lac-Veh, $n = 9$; Lac-THC, $n = 9$). **c**, **d**, Effects of THC on the direct social interaction test on mice treated ICV with saline (**c**, Veh-Sal, $n = 13$; THC-Sal, $n = 16$) or lactate (**d**, Veh-Lac, $n = 13$; THC-Lac, $n = 14$). **, $P < 0.01$ (versus Vehicle). **e**, Overall social exploration through the 3 trials of the direct social interaction task in mice receiving Vehicle (Veh-Sal, $n = 13$; Veh-Lac, $n = 13$) or THC (THC-Sal, $n = 16$; HC-Lac, $n = 14$) under lactate or Saline (total exploration, 3 trials together). *, $P < 0.05$ (versus vehicle). **f**, THC effects (Fig. 4n) on exploration times of social and non-social compartments (Control-Veh, $n = 37$; Control-THC, $n = 38$; NDUFS4-Veh, $n = 10$; NDUFS4-THC, $n = 11$; MCT2-Veh, $n = 15$; MCT2-THC, $n = 13$; mitoCAT-Veh, $n = 11$; mitoCAT-THC, $n = 14$) in mice injected with the different viral vectors. *, $P < 0.05$; **, $P < 0.01$ (versus Non-social). **g**, Locomotor effects of THC administration in the sociability test in mice

injected with the different viral vectors (Control-Veh, $n = 37$; Control-THC, $n = 38$; NDUFS4-Veh, $n = 10$; NDUFS4-THC, $n = 11$; MCT2-Veh, $n = 15$; MCT2-THC, $n = 13$; mitoCAT-Veh, $n = 11$; mitoCAT-THC, $n = 14$). In **f**, **g**, different batches of mice infused with different control viral vectors (Methods) were pooled as One-way ANOVA analysis of social indices in Fig. 4n indicated no statistical differences between control groups ($P = 0.357$). **h**, Representative images of HC and PFC for the different viral vectors infused in HC and PFC. Here, we are showing the expression of mCherry after infusion of AAV2/DJ-CBA-mCherry-miR30E-shMCT2 in these brain regions. **i**, Central (ICV) supplementation of GPR81 receptor agonist (100 nM and 1 mM, $n = 5$) did not rescue the social impairment induced by THC. **, $P < 0.01$ (main effect of THC). **j**, THC effects on the exploration times of social and non-social compartments in the sociability test shown in **i** ($n = 5$). *, $P < 0.05$ (versus non-social). **k**, Locomotor effects of THC administration in the sociability test in mice receiving saline or the GPR81 receptor agonist just before the test ($n = 5$). Data are expressed as mean \pm s.e.m. and are analysed by two-way ANOVA in **a**, **c**, **e**, **f**, **i**, **j**. n represents number of mice. Statistical details, Supplementary Table 2.



Extended Data Fig. 10 | Neuronal expression of mitochondrial catalase in the hippocampus and PFC. Top, immunofluorescence micrographs showing the expression of AAV-hSyn-mitoCAT (fused to mRuby, red) in neurons (staining with an anti-NeuN antibody) or astrocytes (staining with S100- β , green) of HC and PFC. Note the large overlapping in the merged images when using the NeuN antibody (HC, $n = 8$ mice; PFC, $n = 8$) but not the astroglial S100- β marker (HC, $n = 4$ mice; PFC, $n = 4$). Bottom, graph quantification showing the % of mRuby positive cells (neurons) that colocalize with the NeuN antibody. Data are mean \pm s.e.m. Scale bars, 40 μ m.



Extended Data Fig. 11 | Astroglial mtCB₁ receptor activation impairs social interactions by hampering the metabolism of lactate in the brain and altering neuronal functions through a complex I–mROS–HIF-1 pathway.

(1), Activation of astroglial mtCB₁ receptors reduces PKA-dependent phosphorylation of the mitochondrial complex I subunit NDUFS4, which disrupts the assembly and activity of complex I to attenuate the levels of

mitochondrial reactive oxygen species (mROS). (2) The decrease in mROS levels leads to a HIF-1 α -dependent reduction in the glycolytic production of lactate. (3) The diminished release of lactate from astrocytes to neurons through MCT2 results in neuronal bioenergetic and redox stress. All of these processes lead to deficits in social interaction. This scheme was created by the authors with the use of some free images from Servier Medical Art.

Reporting Summary

Nature Research wishes to improve the reproducibility of the work that we publish. This form provides structure for consistency and transparency in reporting. For further information on Nature Research policies, see [Authors & Referees](#) and the [Editorial Policy Checklist](#).

Statistical parameters

When statistical analyses are reported, confirm that the following items are present in the relevant location (e.g. figure legend, table legend, main text, or Methods section).

n/a Confirmed

- The exact sample size (n) for each experimental group/condition, given as a discrete number and unit of measurement
- An indication of whether measurements were taken from distinct samples or whether the same sample was measured repeatedly
- The statistical test(s) used AND whether they are one- or two-sided
Only common tests should be described solely by name; describe more complex techniques in the Methods section.
- A description of all covariates tested
- A description of any assumptions or corrections, such as tests of normality and adjustment for multiple comparisons
- A full description of the statistics including central tendency (e.g. means) or other basic estimates (e.g. regression coefficient) AND variation (e.g. standard deviation) or associated estimates of uncertainty (e.g. confidence intervals)
- For null hypothesis testing, the test statistic (e.g. F , t , r) with confidence intervals, effect sizes, degrees of freedom and P value noted
Give P values as exact values whenever suitable.
- For Bayesian analysis, information on the choice of priors and Markov chain Monte Carlo settings
- For hierarchical and complex designs, identification of the appropriate level for tests and full reporting of outcomes
- Estimates of effect sizes (e.g. Cohen's d , Pearson's r), indicating how they were calculated
- Clearly defined error bars
State explicitly what error bars represent (e.g. SD, SE, CI)

Our web collection on [statistics for biologists](#) may be useful.

Software and code

Policy information about [availability of computer code](#)

Data collection

AMi-maze® interface and ANY-maze® 5.33 software (Stoelting Europe, Dublin, Ireland), CellQuest Pro v5, Clark-type oxygen electrode (Hansatech, UK)

Data analysis

Philips EM208S electron microscope, Digital Morada Camera from Olympus, Variokan Flash (Thermo Fisher, Vantaa, Finland) spectrofluorometer, FACScalibur flow cytometer (BD Biosciences), Nikon Eclipse Ti-E (Tokyo, Japan), Uvikon spectrophotometer (Microbeam S.A., Barcelona, Spain), Mastercycler ep Realplex thermocycler (Eppendorf), Liquid Scintillation Analyzer (Tri-Carb 4810 TR, PerkinElmer), Bruker DPX500 wide-bore spectrometer, epifluorescence Leica DM6000 microscope (Leica, France), Startle chamber (SR-Lab San Diego Instruments, San Diego, USA), AMi-maze® interface and ANY-maze® 5.33 software (Stoelting Europe, Dublin, Ireland).
Softwares: Adobe Photoshop (Adobe Systems, San Jose, CA, USA), Adobe Illustrator CC (Adobe Systems, San Jose, CA, USA), ImageJ 1.48V, CellQuest™ v5, Paint-A-Gate™ PRO (BD Biosciences, New Jersey, USA), FlowJo v10.0.7, GraphPad Prism v8.0 (GraphPad Software Inc, San Diego, USA) IBM SPSS 23.0, Microsoft Excel.

For manuscripts utilizing custom algorithms or software that are central to the research but not yet described in published literature, software must be made available to editors/reviewers upon request. We strongly encourage code deposition in a community repository (e.g. GitHub). See the Nature Research [guidelines for submitting code & software](#) for further information.

Data

Policy information about [availability of data](#)

All manuscripts must include a [data availability statement](#). This statement should provide the following information, where applicable:

- Accession codes, unique identifiers, or web links for publicly available datasets
- A list of figures that have associated raw data
- A description of any restrictions on data availability

The raw data and original gels that support all the figures and findings of this study are available within the Source Data documents or in Supplementary Information.

Field-specific reporting

Please select the best fit for your research. If you are not sure, read the appropriate sections before making your selection.

Life sciences Behavioural & social sciences

For a reference copy of the document with all sections, see [nature.com/authors/policies/ReportingSummary-flat.pdf](https://www.nature.com/authors/policies/ReportingSummary-flat.pdf)

Life sciences

Study design

All studies must disclose on these points even when the disclosure is negative.

Sample size	Sample sizes were decided by the previous experience of the groups in in vitro molecular experiments and in vivo behavioral experiments. Exact information on the sample numbers being analyzed can be found in Figure legends and in Supplementary Information (Tables).
Data exclusions	No data was excluded from the analysis.
Replication	All molecular experiments were repeated from 3 to 5 times, independent biological replicates and the necessary technical replicates for each technique (typically, 4-6 replicas), in order to reproduce the results found. The sample size of the behavioral studies was higher than in the in vitro experiments given the variability in the parameters measured in order to confirm a reliable result. This information has been added in the Statistical section of the manuscript. All attempts at replication were successful.
Randomization	A general method of randomization to assign experimental groups was not performed. Nevertheless, mice in each experimental group were equivalent prior to drug/virus injections.
Blinding	All experiments were done by experienced researchers blind for the experimental conditions.

Materials & experimental systems

Policy information about [availability of materials](#)

n/a	Involvement in the study
<input checked="" type="checkbox"/>	<input type="checkbox"/> Unique materials
<input type="checkbox"/>	<input checked="" type="checkbox"/> Antibodies
<input type="checkbox"/>	<input checked="" type="checkbox"/> Eukaryotic cell lines
<input type="checkbox"/>	<input checked="" type="checkbox"/> Research animals
<input checked="" type="checkbox"/>	<input type="checkbox"/> Human research participants

Antibodies

Antibodies used

Anti-cannabinoid receptor type-1 (CB1) [Frontier Institute Co., Ltd, guinea pig polyclonal; CB1-GP-Af530; AB_2571593]. Mouse monoclonal anti-laminB [B10] (1:100) (sc374015, Santa Cruz Biotechnologies), mouse monoclonal anti- β -actin [AC-15] (1:30,000) (A5441, Sigma, MO, USA), rabbit polyclonal anti-Hsp60 (1:1000; ab46798, Abcam), mouse monoclonal anti- β -ATP [3D5] (1:1,000; MS503, MitoSciences), mouse monoclonal anti-HIF-1 α [241809] (1:1,000; MAB1536, R&D systems), mouse monoclonal anti-complex I Immunocapture [18G12BC2] (1:500) (ab109798, Abcam), rabbit polyclonal anti phospho-(Ser/Thr) PKA substrate (1:1,000) (9621, Cell Signaling), goat polyclonal anti-NDUFS1 (1:500; sc-50132, Santa Cruz Biotechnology), rabbit monoclonal anti-NDUFV2 (1:1,000; ab183715, Abcam), mouse monoclonal S100 β [CL2720] (1:1000, Sigma Aldrich, MO, USA), rabbit polyclonal PHGDH-Rb Af303 (1:500; AB_2571653, Frontier Institute), rabbit polyclonal DsRed (1:1000, Takara Bio Inc, Japan), mouse polyclonal NeuN (1:500, Sigma Aldrich, MO, USA), mouse monoclonal anti-NDUFA9 [20C11B11B11] (1:1,000; ab14713, Abcam), mouse monoclonal anti-NDUFS2 [7A12BE5AD5] (1:800; ab110249, Abcam), mouse monoclonal anti-NDUFB8 [20E9DH10C12] (1:500; ab110242, Abcam), rabbit polyclonal anti-phospho-Ser173 NDUFS4 (1:100) (generously provided by Dr. D. De Rasmio, Bari, Italy) (De Rasmio et al., 2012), and mouse monoclonal NDUFS4 [2C7CD4AG3] (1:800; ab87399, Abcam), rabbit S100 β polyclonal antibody (1:500, Sigma Aldrich, MO, USA), mouse monoclonal anti-GFAP antibody [G3893] (1:1,000, #G3893, Sigma-Aldrich; RRID: AB_477010), goat polyclonal anti-CB1 receptor antibody (2 μ g/ml, #CB1-Go-Af450, Frontier Institute Co.; RRID: AB_257130), goat anti-rabbit IgG, goat anti-mouse IgG or rabbit anti-goat IgG (1:10,000; Santa Cruz Biotechnologies),

Immunoglobulin-G antibody (Fab' fragment, 1:100, Nanoprobes Inc.), avidin-biotin complex (1:50; PK-7100, Vector Labs), fluorescent anti-rabbit Alexa 488 (1:500, Fisher Scientific) secondary antibody, Anti-A522 [EAAT1 (GLAST) Prof. Niels Christian Danbolt University of Oslo; rabbit polyclonal; Ab#314; AB_2314561],

Validation

Anti-phospho-Ser173 NDUFS4 antibody was designed and generously gift by Dr.D. De Rasmio (University of Bari) and validated in his laboratory (PMID: 11705384, PMID: 11852058, PMID: 20303927). All other antibodies used in this study are commercially available and were tested by the manufacturers to recognise the mouse protein in a specific manner.

Eukaryotic cell lines

Policy information about [cell lines](#)

Cell line source(s)

HEK293T (Human Embryonic Kidney Cells). All cell lines were originally obtained from ATCC (CRL-3216, lot number #62729596). This is indicated in the Methods section.

Authentication

The cell line was not authenticate but were used following the instruction of ATCC and following previous experience (Hebert-Chatelain et al. Nature 2016).

Mycoplasma contamination

The cell line used tested negative for mycoplasma contamination from ATCC and this contamination is routinely checked by the users of cell lines.

Commonly misidentified lines
(See [ICLAC](#) register)

Non applicable

Research animals

Policy information about [studies involving animals](#); [ARRIVE guidelines](#) recommended for reporting animal research

Animals/animal-derived materials

Male C57BL/6-N mice purchased from Janvier (France) or bred in the University of Salamanca, CB1-KO male mice bred at the Complutense University of Madrid or in the Neurocentre Magendie (France) and male GFAP-CB1-KO mutant mice and their wild-type (GFAP-CB1-WT) littermates bred at the Neurocentre Magendie were used in this study. The age of the animals at the beginning of all the behavioral experiments was 9-10 weeks. All experimental procedures were approved by the Committee on Animal Health and Care of INSERM and the French Ministry of Agriculture and Forestry (authorization numbers, A501350, A3310035, C33063096) and by the Bioethics Committee of the University of Salamanca in accordance with the Spanish legislation (RD53/2013).

Method-specific reporting

- | | | |
|-------------------------------------|-------------------------------------|----------------------------|
| n/a | <input type="checkbox"/> | Involved in the study |
| <input checked="" type="checkbox"/> | <input type="checkbox"/> | ChIP-seq |
| <input type="checkbox"/> | <input checked="" type="checkbox"/> | Flow cytometry |
| <input checked="" type="checkbox"/> | <input type="checkbox"/> | Magnetic resonance imaging |

Flow Cytometry

Plots

Confirm that:

- The axis labels state the marker and fluorochrome used (e.g. CD4-FITC).
- The axis scales are clearly visible. Include numbers along axes only for bottom left plot of group (a 'group' is an analysis of identical markers).
- All plots are contour plots with outliers or pseudocolor plots.
- A numerical value for number of cells or percentage (with statistics) is provided.

Methodology

Sample preparation

Both mice cortical astrocytes and neurons were used. These cells were treated with the corresponding probes (Mitoxox, DilC1), following manufacturer instructions, during a determined time. After incubation with the corresponding probe, the cells were centrifuged and the pellets were resuspended in PBS for further analysis.

Instrument

FACScalibur flow cytometer (BD Biosciences), equipped with a 15 mW argon laser

Software

the CellQuest™ v5, Paint-A-Gate™ PRO (BD Biosciences) and FlowJo softwares were used for data quantification.

Cell population abundance

For the cytometric analysis, 50,000-100,000 cells were selected in triplicate and by condition.

Gating strategy

The threshold of the analyzer was adjusted in the corresponding channel of the flow cytometer to exclude most subcellular residues or cellular aggregates. With this, background noise was estimated due to the rupture of neurites and cell extensions, and doublets or triplets formed by intercellular junctions

- Tick this box to confirm that a figure exemplifying the gating strategy is provided in the Supplementary Information.